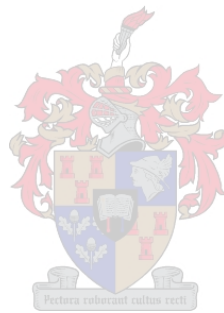# A matter of life or death: autophagy in the context of prolonged doxorubicin therapy

by

Muneeb Adonis

Supervisor: Dr Balindiwe Sishi

Thesis presented in fulfilment of the requirements

for the degree of

Master of Science (Physiological Sciences)

in the Faculty of Science

at Stellenbosch University

April 2019

Declaration

By submitting this thesis electronically, I declare that the entirety of the work contained therein is my own, original work, that I am the sole author thereof (save to the extent explicitly otherwise stated), that reproduction and publication thereof by Stellenbosch University will not infringe any third-party rights and that I have not previously in its entirety or in part submitted it for obtaining any qualification.

April 2019

Abstract

Introduction

Doxorubicin (DOX) is an effective treatment against a variety of cancers, and thus remains a commonly used chemotherapeutic drug. The chief side effect of DOX treatment is cardiotoxicity. The precise mechanisms by which DOX induces cardiotoxicity are unknown. One of the most accepted mechanisms is the excess production of ROS. The structure of DOX allows it to undergo redox cycling and form DOX-iron complexes, both of which generate free radicals. DOX-induced oxidative damage is more prevalent in the heart than other organs. As the pathogenesis of cardiotoxicity appears to be mediated by oxidative stress, it seems as if the most effective treatment would be antioxidant therapy. Antioxidant therapy has proved unsuccessful. Autophagy is a catabolic process which allows a cell to remove cytoplasmic components. Components regarded as surplus or defective may be removed to ensure the survival of the cell. There have been numerous studies conducted to evaluate the relationship between DOX and autophagy. Many of these studies have concluded that DOX treatment does affect autophagy. Although there is literature to support both the up and downregulation of autophagy. We hypothesis that during the development of DOX-induced cardiotoxicity autophagy is downregulated. Attenuation of this downregulation during DOX therapy will attenuate the effects of cardiotoxicity.

Methodology

Three-week-old male black 6 (C57BL/6) mice were split into six groups; vehicle control, DOX, rapamycin, a starvation, DOX and rapamycin combination and DOX and starvation group. The DOX group received 2mg/kg DOX weekly for a total of eight weeks, resulting in a cumulative dose of 16mg/kg. The rapamycin group received 2mg/kg rapamycin weekly. The DOX and rapamycin group received rapamycin 30 minutes prior to receiving DOX. The starvation group was starved from food for 24 hours each week but were allowed free access to drinking water. The DOX and starvation group were starved for 24 hours prior to receiving DOX. A week after the final treatment, mice were euthanised. The whole hearts were harvested and sectioned, roughly into halves. One half of each was stored in formaldehyde solution for histological analysis, the other was frozen in liquid nitrogen for biochemical analysis. H&E staining was performed to assess tissue morphology and cardiomyocytes area. Picrosirius red staining was performed to assess fibrosis. Fluorometry was done to assess oxidative stress via GSH, GSSG

and CDs levels. Western blots were performed to assess expression of caspase 3 and LC3. A Kolmogorov- Smirnov normality test was done to test for a normal distribution. Appropriate statistical tests were applied. P-values were considered significant when $P < 0.05$.

Results

Differences in body mass first appeared at week 5, with both DOX+ Rapa and DOX+ starve weighing less than control. Differences then appeared (at week 6) between DOX and control, with DOX weighing less than control. These differences continued until the end of the study. Histology showed cardiomyocyte area was decrease in the DOX group (97.4± 4.1) the control (112.6± 4.3). There was also an increase in fibrosis in the DOX group (2.07± 0.22) compared to the control (1.05± 0.18) and the DOX+ starve group (1.21± 0.18) had less fibrosis than DOX alone. Biochemical analysis showed autophagy was decreased in the DOX group (0.3733± 0.0683) compared to the control group (1.1420± 0.2262). However, the DOX+ Rapa (0.4344± 0,0543) and DOX+ starve (0.4818± 0.1240) groups also had decreased autophagy compared to the control group.

Discussion

The histological analysis confirms cardiotoxicity as DOX caused cardiac damage. Biochemical analysis was less straightforward. Oxidative stress markers were tested for too long after levels may have been detectable. While this provides no oxidative stress data, it suggests the cardiotoxicity was chronic rather than acute, as cardiac damage persisted after the stress had ended. Apoptotic data was inconclusive. DOX treatment caused a decrease in autophagy. Meaning, as hypothesised, this could be the target of an adjuvant therapy. The adjuvant treatment groups showed some improvement when compared to the DOX group. Both the DOX+ Rapa and DOX+ starve group showed histological improvement. The LC3 data however showed, the adjuvant therapies did not upregulate autophagy. Neither DOX+ Rapa nor DOX+ starve showed any increases in autophagy when compared to DOX. Due to the lack of attenuation of autophagic dysregulation, the reason for the protective effect of the adjuvant therapy is a mystery. Regardless, this study suggests that autophagic upregulation a potential adjuvant therapy.

Uittreksel

Inleiding

Doksorubisien (DOX) dien as 'n effektiewe behandelingsmiddel in onkologie en sodoende 'n fundamentele chemoterapeutiese middel wat teen 'n verskeidenheid kankers gebruik word. Die kliniese gebruik hiervan word beperk deur die kumulatiewe dosis afhangklike newe effekte wat maande, jare en selfs dekades na behandeling aanleiding kan gee tot die ontstaan van hartversaking. Daar word voorgestel dat kardiotoksisiteit, wat die hoof newe effek is wat met doksorubisien toediening geassosieer word, gerig is op oormatige ROS produksie wat 'n toestand van oksidatiewe stres veroorsaak en gevolglik seldood as 'n afstroom effek veroorsaak. Dit is verder bekend dat die chemiese struktuur van DOX betrokke is in resirkulering en die vorming van DOX-yster komplekse wat beide vryradikale kan produseer. Omrede die hart energie moet produseer om aan sy funksionering te kan voldoen in hierdie hoë oksidatiewe omgewing met lae anti-oksidant beskerming, word regenerasie kapasiteit ingeperk. Dit is dus verstaanbaar hoekom hierdie orgaan vatbaar is vir oksidatiewe stress. Hoewel kardiotoksisiteit geklassifiseer kan word as akute- en chronies stadium, is daar beperkte behandelingsopsies of ondersteuningsterapie om hierdie vertraging van newe effekte te voorkom. Outofagie, 'n evolusionêre konserveringsproses van proteïendegradasie, het voorheen in verskeie kardiovaskulêre patologieë beskerming getoon. Daar is ook verskeie teenstrydige bewyse in die literatuur oor die rol van DOX en outofagtiese aktiwiteit; dit is nie duidelik of die onaktiewiteit daarvan bydra tot kardiotoksisiteit en/of die aktiwiteit beskerming bied nie. Hierdie studie ondersoek dus die potensiële beskermings effekte van outofagiese opregulering in 'n rotmodel met verlengde DOX behandeling.

Metodologie:

Nadat etiese goedkeuring vir die studie verleen is, is drie week oue manlike swart 6 (C57BL/6) muise ontvang en ewekansig verdeel in ses eksperimentele groepe na klimatisering. Hierdie groepe sluit in: 'n kontrole (draer), rapamisien, uithongering, DOX en kombinasies van DOX met rapamisien of uithongering. Terwyl die DOX en rapamisien groepe 2 mg/kg DOX of rapamisien weekliks ontvang het, is die uithongeringsgroep 24 uur weerhou van voedsel. In die kombineringsgroep is rapamisien 30 minute voor DOX behandeling toegedien, wat vooraf met 'n 24 uur uithongeringsperiode vooraf gegaan is voordat chemoterapeutiese behandeling begin is. Die behandelingsprotokol is vir agtweke volhou met alle toedienings intraperitoneaal

gelewer. Een week na die finale toediening is die muise met behulp van eutanasie dood gemaak waarna die harte verwyder is. Een helfte van die hart is in formaldehiedoplossing vir histologiese evaluasie geberg, en die ander helfte gevries in vloeibare stikstofvir biochemiese analises. Om die morfologiese wysigings te ondersoek asook ontwikkeling van fibrose is 'n H&E en Picrosirius rooikleuring uitgevoer. Anti-okisdant status en oksidatiewe skade is bepaal deur veranderinge in die gereduseerde versus geokssideerde glutatioonverhouding en die teenwoordigheid van gekonjugeerde diëne onderskeidelik. Ten slotte is apoptose bepaal deur die uitdrukking van kaspase-3 vlakke. Gepaste statistiese toetse is gebruik waar $p < 0.05$ as betekenisvol beskou is.

Resultate

Verskille in die liggaamsmassa is beduidend teen die vyfde week met DOX behandeling en die outofagiese opregulering het geen bydrae gelewer tot hierdie verlies aan massa nie. Geen verandering in miokardiale massa is waargeneem by enige van die behandelingsgroepe nie. Daar is wel betekenisvolle fibrose ($2.07\pm0.22\%$, $p < 0.001$) met 'n afname in miobrillêre area (97.41 ± 4.1 μM^2, $p < 0.01$) in die DOX behandelings groepe versus die kontrole ($1.05 \pm0.18\%$ fibrose, 112.6 ± 4.32 μM^2) opgemerk. Vergeleke met die DOX groep, het die kombineringsgroep verlaagde fibrose in uithongering getoon ($1.21\pm0.18\%$, $p < 0.01$) en 'n matige toename in miofibrillêre area is waargeneem. Verbasend is daar geen veranderinge waargeneem in die oksidatiewe stresparameters en induksie van apoptose nie. Hierdie studie het suskesvol demonstreer dat DOX 'n kragtige inhiberings effek op outofagie het omrede beide intervensies wat gebruik is om die aktiwiteit te stimuleer onsuksesvol was om hierdie toestand te handhaaf in die teenwoordigheid van DOX.

Bespreking

Hierdie studie het die terapeutiese potensiaal van verhoogde outofagie deur farmakologiese (rapamisien) en 'n fisiologiese (uithongering) benadering ondersoek in 'n poging om die newe effekte wat met DOX terapie in die hart geassosiëer word te verlaag. Hoewel die model wat hier gebruik is uniek is en wel sekere eienskappe vertoon het, hoofsaaklik fisies (liggaamsmassa) en struktureel (miofibrillêre area en fibrose); het die biochemiese parameters (oksidatiewe stres en apoptose) onoortuigende resultate opgelewer. Hoewel die resultate van ons studie veronderstel dat strukturele modifikasies aanvang neem voordat biochemiese veranderinge onstaan, kan daar geen defnitiewe afleidings gemaak word oor die die impak van terapeutiese intervensie in hierdie scenario nie.

Acknowledgements

I would like to thank the following individuals:

Firstly, my supervisor Dr Balindiwe Sishi for giving me the opportunity to come to Stellenbosch University and pursue an M.Sc. Thank you for providing me with a wonderful project, one which I am deeply passionate about. Your patience, support and guidance has helped me grow not only as a scientist but also as a person.

The NRF for providing funding for this project.

Dr Theo Nell, for translating my abstract into Afrikaans.

Judy Farao and Tracey Ollewagen for your assistance and company in the animal house. Without your help, I would not have been able to manage looking after all those tiny mice and perform the numerous tests needed for this project.

Reggie Williams of the Anatomy & Histology Division of the Biomedical Department, Faculty of Medicine & Health, Tygerberg Campus. Your expertise and intuition guided me through some tricky histological problems.

Fanie Rautenbach of the Oxidative Stress Research Centre, CPUT, Bellville Campus. Your patients, professionalism and knowledge were a great help as we worked through some challenging oxidative stress assays.

CORG for the constant support. Each individual member has helped me in a unique way during this project. With too many names and specific incidents to mention. Whether it be profession or personal assistance, this group was always there to help.

And lastly, DSG and the Department of Physiological Sciences in general. Your warm welcome has made me feel at home in the department, quickly calming any nerves I had about changing institutions and helping me adjust to my new environment.

Table of Contents

List of Abbreviations

3-MA   3-methyladenine

9-COOH   9-dehydroxyacetyl-9-carboxyl

ABCB8   adenosine triphosphate -binding cassette subfamily B member 8

AIF   apoptosis inducing factor

AMCM   adult mouse cardiomyocytes

AMPK   adenosine monophosphate-activated protein kinase

ANOVA   analysis of variance

ARCM   adult rat cardiomyocytes

Atg   autophagy related

ATP   adenosine triphosphate

APS   astragalus polysaccharide

BAF- A1   bafilomycin- A1

C   carbon

C57BL/6   black 6 mice

Ca^2 calcium ion

CD   cumulative dose

CDs   conjugated dienes

CMA   chaperone mediated autophagy

Cpd C   AMPK inhibitor compound C

dH_2O deionized water

DNA   deoxyribose nucleic acid

DOX   doxorubicin

E1   ubiquitin-activating enzyme

E2   ubiquitin conjugation enzyme

E3   ubiquitin protein ligase

ECL   enhanced chemiluminescent

ECG   electrocardiography

ECM   extracellular matrix

EDTA   ethylenediaminetetraacetic acid

eNOS	endothelial nitric oxide synthase
ERK	extracellular signal regulated kinases
FDA	food and drug administration
Fe^{2+}	iron (II)
Fe^{3+}	iron (III)
FKBP12	FK506 binding protein
FoxO	forkhead box
GAPDH	glyceraldehyde 3-phosphate dehydrogenase
GSH	glutathione
GSSG	glutathione disulphide
H&E	haematoxylin and eosin
H_2O	water
H_2O_2	hydrogen peroxide
H9c2	rat heart myoblast
HDAC6	histone deacetylase 6
HF	heart failure
IP	intraperitoneal
I/R	ischemia reperfusion
KS	Kolmogorov- Smirnov normality test
LAMP-2A	lysosome-associated membrane protein 2
LC3	light chain 3
LF PVDF	low-fluorescence polyvinylidene fluoride
LKB1	liver kinase B1
LSD	least squared differences
LVEF	left ventricular ejection fraction
M2VP	1-methyl-2-vinylpyridinium triflate phosphate
MAC	mitochondrial apoptosis-inducing channel
MCL	mantle cell lymphoma
MDA	malondialdehyde
MIR	mid- infrared

miR-30a	micro ribonucleic acid 30a
mitoKATP	mitochondrial potassium ATP
MPT	mitochondrial permeability transition
mRNA	micro ribonucleic acid
mTOR	mammalian target of rapamycin
mTORC1	mammalian target of rapamycin complex 1
mTORC2	mammalian target of rapamycin complex 2
MuRF-1	muscle RING Finger 1
n	sample size
NBR1	neighbour of BRCA1 gene 1 protein
NADH	nicotinamide adenine dinucleotide
NADPH	nicotinamide adenine dinucleotide phosphate
NEC	neuroendocrine carcinoma
NMCM	neonatal mouse cardiomyocytes
NRCM	neonatal rat cardiomyocytes
NSCLC	non-small cell lung cancer
O_2	oxygen
O_2-	superoxide anions
OH	hydroxyl radicals
PAH	pulmonary arterial hypertension
PARP	poly adenosine diphosphate-ribose polymerase
PAS	phagophore assembly site
PE	phenylephrine
PI3-K	phosphoinositide 3-kinases
PKB/ Akt	protein kinase B
PNET	progressive neuroendocrine tumours
PTEN	phosphatase and tensin homolog
PTFE	polytetrafluoroethylene
Rapa	rapamycin
RCC	renal cancer carcinoma

RIPA	radioimmunoprecipitation assay
ROS	reactive oxygen species
RTA	ready to assemble
RTK	receptor tyrosine kinase
SEM	standard error of the mean
SGK1	serum and glucocorticoid-regulated kinase 1
Smac	second mitochondria-derived activator of caspases
TBS-T	tris buffered saline with tween 20
TAC	transverse aortic constriction
Top2	topoisomerase II
TSC	tuberous sclerosis proteins
Ub	ubiquitin
ULK	unc-51 like autophagy activating kinase
UPP	ubiquitin proteasome pathway
UVRAG	ultraviolet radiation resistance-associated gene protein
WHO	world health organization

List of Units of Measurement

Arbitrary units	AU
Degrees Celsius	°C
Grams	g
Kilodaltons	kDa
Kilograms	kg
Litres	L
Meters squared	m²
Micrograms	µg
Microlitres	µL
Micrometres	µm
Micrometres squared	µm²
Micromoles	µMol
Milligrams	mg
Millilitres	mL
Millimetres squared	mm²
Millimoles	mMol
Moles	Mol
Nanometres	nm
Percentage	%
Rotation Per Minute	RPM
Voltage	V

List of Figures

List of Tables

Chapter 1: Literature Review

1.1. Anthracycline chemotherapy

Anthracycline antibiotics are a class of chemotherapeutic antibiotics, first isolated from Streptomyces cultures in the late 1950s in laboratories across the globe (Muggia & Green 1991). Doxorubicin (DOX), an anthracycline first isolated in the early 1960s from *Streptomyces peucetius* bacteria, is an effective treatment against a variety of cancers, listed in Table 1.1 (Arcamone et al. 1969; Tacar et al. 2012). Due to its effectiveness DOX remains a commonly used chemotherapeutic drug and is even listed by the World Health Organisation (WHO) on their model list of essential medicines (Tacar et al. 2012; World Health Organization 2017).

Table 1.1: Table listing DOX treated cancers, adapted from Tacar *et al*, 2012

Adrenal cortex cancer	Multiple myeloma
Bone cancer	Pancreatic cancer
Breast cancer	Prostate cancer
Cervical, endometrial, uterine and womb cancer	Skin, mucous membrane cancer
Head and neck cancer	Soft tissue cancer e.g. leiomyosarcoma
Lung cancer	Stomach cancer

1.2. Anti-cancer Mechanisms of action

Despite its wide use, the precise mechanisms of action of DOX's chemotherapeutic effects are still under debate. There have been several proposed mechanisms, each with merit. Some of the proposed mechanisms include the generation of free radicals, the inhibition of deoxyribose nucleic acid (DNA) synthesis and direct membrane binding. Free radical generation results in increased oxidative stress, causing the induction of lipid peroxidation as well as DNA damage (Keizer et al. 1990). DNA synthesis is inhibited by the formation of DOX-DNA adducts, the disruption of DNA unwinding, strand separation, helicase and topoisomerase II activities and transcription (Goodman *et al*, 1974; Gewirtz, 1999; Cutts *et al*, 2005).

Of the many proposed mechanisms, the two most probable appear to be the generation of free radicals and the inhibition of topoisomerase II activity. These two mechanisms are the most cited and relevant, not only in the context of cancer therapy but also in the context of cardiovascular disease (Keizer *et al*, 1990; Ghigo *et al*, 2015).

1.2.1.1. Redox cycling

The structure of DOX allows it to act as an electron acceptor and thus undergoes redox cycling to generate free radicals (Goodman *et al*, 1974). Structurally, as indicated in Figure 1.1 A, DOX has aglyconic and sugar moieties. The tetracyclic ring makes up the aglyconic moiety and the sugar moiety, attached at carbon (C)-7, consists of a 3-amino-2,3,6- trideoxy-L-fucosyl moiety called daunosamine. This unique feature is understood to be responsible for antineoplastic and cardiotoxic effects. There is a methoxy substituent at C-4. Quinone groups are present on C-5 and C-12 and hydroquinone groups are present on C-6 and C-11 respectively. Finally, a primary alcohol side chain located at C-9 differentiates DOX from other anthracyclines. A carbonyl is present at C-13. (Minotti *et al*, 2004).

Reduction of the quinone groups on the C ring, catalysed by nicotinamide adenine dinucleotide (NADH), nicotinamide adenine dinucleotide phosphate (NADPH) or cytochrome P-450 reductase, converts the quinones to semiquinone free radicals. These semiquinone free radicals are then oxidised by donating an electron to oxygen (O_2), thus generating superoxide anions (O_2-) and other reactive oxygen species (ROS) such as hydrogen peroxide (H_2O_2). This reaction, indicated in Figure 1.1 B is cyclic and can generate large amounts of free radicals. (Keizer *et al*, 1990; Minotti *et al*, 2004).
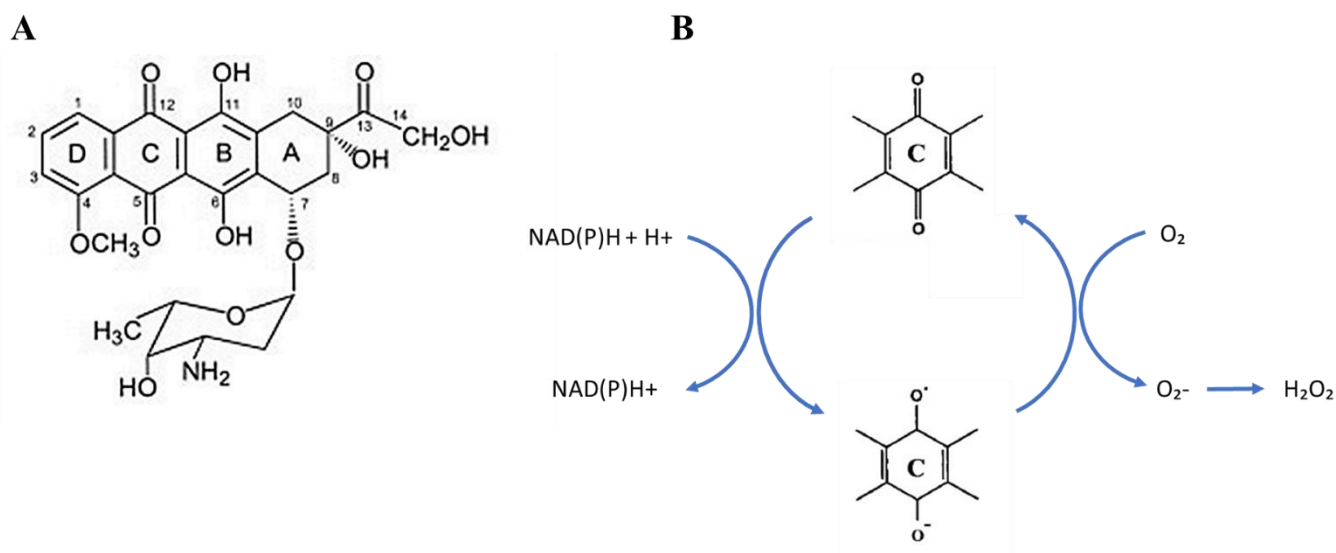
Figure 1.1 A: Diagram displaying the structure of DOX. B: Redox cycling of the quinone groups on the C ring, converting quinones to semiquinone free radicals. Semiquinone free radicals are oxidised by donating an electron to O_2, generating O_2- and H_2O_2. Adapted from Minotti *et al*, 2004

1.2.2. Iron complexes

DOX also forms free radicals through the reduction of DOX-iron complexes. The two main mechanisms of DOX-iron complex free radical formation are indicated in Figure 1.2, one dependent (Figure 1.2 red) and one independent of a reducing system (Figure 1.2 green).

In the presence of a reducing system, DOX-iron(III) (DOX-Fe^{3+}) complex is reduced to DOX-iron(II) (DOX-Fe^{2+}) (by NADPH or cytochrome P-450 reductase or glutathione). DOX-Fe^{2+} is then oxidised by donating an electron to O_2. As with the redox cycling previously described, this reaction is cyclic and generates ROS (Zweier, 1984). H_2O_2 can react with DOX-Fe^{2+} to form hydroxyl radicals (OH).

In the absence of a reducing system DOX-Fe^{3+} can reduce chelated iron by two separate intramolecular redox reactions. Either by oxidation of the hydroquinone moiety at ring B or the oxidation of the C-9 side chain. This forms the DOX-Fe^{2+} complex which is oxidized to generate free radicals. Further oxidation of the C-9 side chain leads to the formation of the oxidized metabolite of DOX, 9-dehydroxyacetyl-9-carboxyl doxorubicin (9-COOH-doxorubicin) (Zweier *et al*, 1986). This leads to DNA damage, lipid peroxidation and ultimately destruction of the cell (Muindi *et al*, 1984; Keizer *et al*, 1990).

3
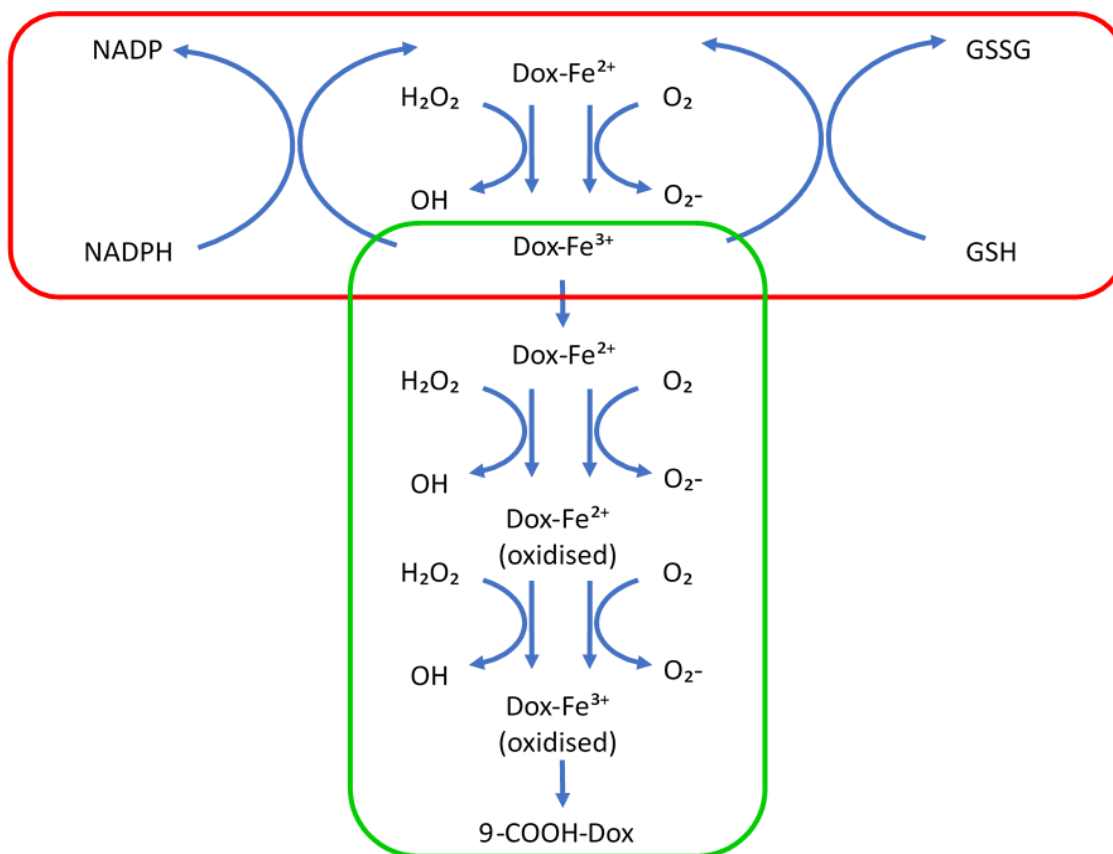
Figure 1.2: Iron complex free radical formation in the presence of a reducing system, DOX-Fe^{3+} complex is reduced to DOX-Fe^{2+}, then oxidised by donating an electron to O_2, H_2O_2 also reacts with DOX-Fe^{2+} to form OH (red). In the absence of a reducing system, DOX-Fe^{3+} can reduce its chelated iron by two redox reactions, oxidation of the hydro-quinone moiety at ring B or the oxidation of the C9 side chain. This forms the DOX-Fe^{2+} which is oxidized to generate free radicals. Oxidation of the C9 side chain leads to the formation of the oxidized metabolite of DOX, 9-COOH-doxorubicin (green). Adapted from Keizer *et al*, 1990.

1.2.3. Topoisomerase II

Another widely supported mechanism of action for DOX is its ability inhibit topoisomerase II (Top2) activity. Top2 is an enzyme consisting of alpha (α) and beta (β) isoforms. Both isoforms are present in mammalian cells and are essential for cell replication. During DNA replication Top2 induces double strand breaks and then covalently binds proteins to the broken ends to prevent rearrangement or illicit a DNA damage response. This mechanism helps uncoil the DNA, allowing replication to take place. Following DNA replication, Top2 also assists in chromatid condensation and prevents early chromatid separation during mitosis. Additionally, Top2 assists in transcription activation. Cell machinery monitors the activity of Top2 and uses its various functions as checkpoints to monitor the cell cycle and allow replication to take place. Defective functioning of Top2 would be detected by the cell machinery and lead to the destruction of the defective cell (Nitiss, 2009).

DOX inhibits Top2 function by forming a stable Top2-DNA complex. The two central B and C rings of DOX overlap with adjacent DNA base pairs and the D ring passes through the intercalation site of the Top2-DNA complex forming a stable adduct. This DOX-Top2-DNA complex is formed after the double strand break and thus prevents DNA from resealing thus eliciting a DNA damage response which leads to apoptosis (Tewey *et al,* 1984; Minotti *et al,* 2004).

1.3. Cardiotoxicity

Like many medications, DOX has unwanted side effects, chief of which is cardiotoxicity (Lefrak *et al,* 1973). Cardiotoxicity is a broad term used to define any toxicity that affects the heart. This definition, however, is vague and may apply to any toxin affecting the heart. This had led to some debate about whether certain cardiac pathologies may be linked to chemotherapy. Subsequently, chemotherapy-induced cardiotoxicity has been clinically defined by the cardiac review and evaluation committee supervising trastuzumab (breast cancer chemotherapeutic) clinical trials. According to this committee chemotherapy-induced cardiotoxicity is defined as one or more of the following;

- signs or symptoms of heart failure (HF)
- a reduction in left ventricular ejection fraction (LVEF) globally or in the interventricular septum specifically
- a reduction in LVEF between 5% and 55% in the presence of signs or symptoms of HF
- a reduction in LVEF between 10% and 55% in the absence signs or symptoms of HF (Seidman *et al,* 2002; Florescu *et al,* 2013).

There is evidence, dating back to the late 1970s, to support a dose-response relationship between DOX and the increased risk of cardiotoxicity (Von Hoff *et al,* 1979). This study found a 3% risk of cardiotoxicity at a cumulative dose of 400 mg/m², 7% at 550 mg/m² and 18% at 700 mg/m². Thus, it was concluded to limit DOX to a cumulative dose of less than 550 mg/m². However, while this number is still considered by many to be the upper limit for DOX exposure, subsequent studies have suggested this limit to be much lower. Swain *et al,* 2003 found that the risk of developing cardiotoxicity to be 5% at 400 mg/m², 26% at 550 mg/m² and 48% at 700 mg/m². Based on these estimates it was suggested to further reduced the limit of DOX to a cumulative dose of no more than 400 mg/m². The difference is most likely due to the unclear definition of DOX-induced cardiotoxicity and more specifically, the numerous risk

factors associated with the increased risk of developing cardiotoxicity such as age, gender, underlying cardiovascular abnormalities or previous chemotherapeutic treatment. This underlines the need for stricter definitions, standards and guidelines. Regardless, while limiting the dose of DOX reduces the risk of cardiotoxicity, it is not completely effective at preventing this pathology as cardiotoxicity may still develop even at lower doses. Patients suffering from DOX-induced cardiotoxicity are broadly classified into two types; acute or chronic.

1.3.1. Acute cardiotoxicity

The acute form of cardiotoxicity, associated with cardiomyocyte dysfunction, develops either during treatment or a few hours/days thereafter. There are a wide variety of symptoms including; electrocardiograph (ECG) changes (particularly ST-T changes) and cardiac arrhythmias (particularly sinus tachycardia). Inflammatory responses such as pericarditis or myocarditis do occur although they are less common. This form of cardiotoxicity is clinically manageable and is dose-independent. Treatment of the individual symptoms tends to resolve the condition without lasting damage (Lefrak *et al,* 1973; Bristow *et al,* 1978; Frishman *et al,* 1996; Florescu *et al,* 2013).

1.3.2. Chronic cardiotoxicity

The chronic form, associated with cardiomyocyte death, develops months or even years after treatment. There are a wide variety of physiological symptoms including atrophy, chamber dilation, fibrosis and overall functional decline, particularly of the left ventricle. This functional decline may progress to congestive heart failure and ultimately death (Frishman *et al*, 1996). Biopsies reveal histological damage including cardiac tissue containing cells with abnormal nuclei, severe mitochondrial damage, partial or complete myofibril loss (which leaves only remnants of peripheral Z disks) and vacuolar degeneration (characterised by swelling and merging of vacuoles). Unlike the acute form, there are currently no effective therapies to treat chronic cardiotoxicity, resulting in permanent damage (Takemura & Fujiwara, 2007; Vejpongsa & Yeh, 2014).

In contrast to acute cardiotoxicity, chronic cardiotoxicity is does-dependent and causes irreversible damage to the myocardium. As such, there are currently no effective therapies to treat this condition, other than a heart transplant (Vejpongsa & Yeh, 2014). Since this condition

takes years to manifest, it is difficult to determine he main mechanisms involved, although a few have been proposed.

1.3.3. Proposed mechanisms of cardiotoxicity

The precise mechanisms of action for DOX-induced cardiotoxicity are unknown. One of the long-standing theories suggested to be responsible for DOX-induced cardiotoxicity is the oxidative stress hypothesis. This is due to the ability of DOX to generate elevated levels of free radicals (Olson *et al,* 1981), as previously mentioned. Furthermore, the heart is more susceptible to oxidative damage than other organs.

As the myocardium is a muscle which is constantly active, it requires a great deal of energy. To cope with this high demand of adenosine triphosphate (ATP), cardiac tissue contains a greater number of mitochondria than most tissues. DOX is known to have a high affinity for cardiolipin, a phospholipid found in the inner mitochondrial membrane, binding and forming a strong complex with cardiolipin, resulting in accumulation of DOX in the mitochondria (Goormaghtigh *et al,* 1980). This accumulation of DOX in the mitochondria in turn leads to iron accumulation in the mitochondria. DOX reduces the levels of ATP-binding cassette sub-family B member 8 (ABCB8), a protein which regulates mitochondrial iron export. It also increases mitochondrial ferritin, an iron storage protein. This prevents iron from exiting the mitochondria, causing it to build up within the organelle, leading to formation of ROS within the cardiac mitochondria through reduction of the quinone groups on the C ring and reduction of DOX-iron complexes, as previously mentioned. In addition, there is also a reduction of endothelial nitric oxide synthase (eNOS) and NADPH, although these contribute relatively small amount of ROS (Ichikawa *et al,* 2014). The localised increase in oxidative stress as well as the relatively low levels of antioxidants in the heart results in apoptosis of cardiomyocytes. Apoptosis is believed to be the cause of the severe damage associated with chronic cardiotoxicity (Octavia *et al,* 2012).

1.3.4. The role of apoptosis

Apoptosis is a form of programmed cell death. Carefully regulated signal cascades lead to the packaging of cytoplasm, cellular organelles and nuclear fragments into small vesicles called apoptotic bodies. These apoptotic bodies are phagocytosed, removing the cell with little disturbance to the surrounding tissue (Kerr *et al,* 1972). There are two processes which induce

apoptosis, the extrinsic and intrinsic pathways. The extrinsic pathway is initiated by extracellular ligands binding to surface receptors on the cell, while the intrinsic pathway is initiated by intracellular signals.

DOX induces apoptosis primarily through the intrinsic pathway. DOX treatment inhibits protein kinase B (PKB/ Akt) signalling, resulting in the upregulation of the pro-apoptotic protein, Bad. The ROS generated by DOX treatment damages DNA and causes calcium ion (Ca^{2+}) dysregulation. DNA damage leads to an increase in both the expression and activation of the tumour suppressor protein, p53. p53 then upregulates the pro-apoptotic protein, Bax, which localizes at the mitochondrial membrane, opening the mitochondrial apoptosis-inducing channel (MAC). ROS increases intracellular Ca^{2+} levels by releasing Ca^{2+} from the endoplasmic reticulum. This increase can generate ROS through calcium-sensitive ROS-generating enzymes. This leads to an increase in mitochondrial Ca^{2+} which, once increased beyond threshold, causes the opening of the mitochondrial permeability transition (MPT) (Zhang *et al,* 2009). The net effect of these stimuli is the opening of mitochondrial membrane pores, leading to pro-apoptotic proteins leaking out of the mitochondrial intermembrane space and into the cytoplasm. These proteins include apoptosis inducing factor (AIF), second mitochondrial-redived activator of caspases (smac), cytochrome C, endonuclease G and omi/HtrA2. These proteins then aid in the formation of the apoptosome, activation of initiator caspase-9 and executioner caspase-3, which cleaves cellular components which are then packaged into apoptotic bodies and phagocytosed (Elmore, 2007).

1.4. Current therapies

1.4.1. Antioxidants

As the pathogenesis of cardiotoxicity appears to be mediated by oxidative stress, it seems as if the most effective treatment would be antioxidant therapy. A meta-analysis of randomised controlled trials was conducted to analyse the efficacy of vitamins A, B6, B12, C, D, E and antioxidant therapy on cardiac disease progression. While pre-clinical trials such as *in vitro* and *in vivo* studies showed that vitamin and antioxidant therapies can hinder the progression of certain cardiac pathologies, including cardiotoxicity, clinical studies have demonstrated little to no protective effects (Myung *et al,* 2013; Sterba *et al,* 2013).

Many theories have been proposed as to why antioxidant therapies suddenly become ineffective in the clinical setting. The dose, duration, frequency and choice of antioxidant have all come into question (Steinhubl, 2008). Antioxidants may also not be effective as they may be unable to reach their intended target within the cell. The oxidative stress associated with cardiotoxicity occurs at the mitochondrial level. Many antioxidants are unable to reach the mitochondria and are therefore unable to scavenge the ROS damaging the cell. It may be necessary for antioxidants to be specifically targeted to the mitochondria in order for them to prove effective in the clinical setting. Another potential reason for the ineffectiveness of antioxidants may be that oxidative stress is only one of the factors causing cardiotoxicity. Therefore antioxidants are only effective against one of the many causes of the disease (Murphy & Smith, 2000; Adlam *et al,* 2017).

1.4.2. Iron chelators

Iron chelators have shown more promise in the clinical setting. Dexrazoxane, an iron chelator similar to ethylenediaminetetraacetic acid (EDTA), is used as an adjuvant therapy to limit cardiotoxicity. Unlike the water soluble EDTA, dexrazoxane is lipid soluble and can easily transverse the cell membrane and enter cells. It is then able to dissociate iron from the DOX-Fe complexes. This elicits a cardioprotective effect, as shown by Marty *et al,* 2006. In this study women who received dexrazoxane prior to anthracycline treatment were significantly less (68%) likely to develop cardiac dysfunction compared to those who received anthracyclines alone.

However, dexrazoxane, like all medication, has side effects. Dexrazoxane may cause pain or superficial phlebitis at the injection site, thus it is recommended that it is infused into a large vein. Alopecia, mucositis, nausea and vomiting are common in patients treated with dexrazoxane. These symptoms are similar to anthracycline toxicity, making it difficult to differentiate the cause. At near maximum doses, dexrazoxane treatment has been linked to increased levels of iron and zinc in urine, reversible liver dysfunction (elevated alanine aminotransferase/ aspartate aminotransferase) and more seriously, myelotoxicity (bone marrow suppression). Long term effects are also not fully understood with a potential threefold increase in second primary malignancies (acute myeloid leukemic/myelodysplastic syndrome). The findings have led to restrictions for dexrazoxane as a cardiotoxicity treatment in Europe (Langer, 2014). Due to the limitations of the current treatments, it is essential to find better but effective adjuvant therapies.

1.5. Autophagy

Autophagy is a complex catabolic process which allows a cell to remove specific cytoplasmic components. Under specific stresses (such as starvation) certain cellular organelles and proteins may be regarded as surplus or defective and destroyed to ensure the survival of the cell (Yang *et al,* 2013). The macromolecules generated from autophagy are recycled allowing the cell to reuse the molecules again under more favourable conditions. First discovered in the early 1960s in rat liver, it was observed that following perfusion with glucagon, an increase in lysosomal activity was observed. These lysosomes contained mitochondria, safely removing the organelle from the cell under stressful conditions (Ashford & Porter, 1962).

There are three distinct kinds of autophagy, namely: macro-autophagy, micro-autophagy and chaperone-mediated autophagy (CMA) (Kobayashi, 2015). Macro-autophagy involves the formation of a double membrane-bound vesicle, termed an autophagosome, delivering cytoplasmic components to a lysosome, fusing with the lysosome to form an autolysosome, which then degrades the cargo. During micro-autophagy, cytosolic components are directly engulfed by the lysosome through invagination of the lysosomal membrane. Both macro and micro-autophagy are able to engulf large cytoplasmic components through selective or non-selective mechanisms. During CMA, targeted cytosolic components are marked with chaperone proteins which are recognised by the lysosomal membrane receptor lysosomal-associated membrane protein 2A (LAMP-2A). This protein complex is translocated across the lysosomal membrane resulting in degradation (Glick *et al,* 2010). All uses of the term 'autophagy' from this point onward are in reference to macro-autophagy.

1.5.1. Mechanism

The mechanism of autophagy is regulated by autophagy related (Atg) proteins. It follows a process that can be divided into a few steps; induction, autophagosome formation, autophagolysosomal formation and finally degradation of the cellular components (Yang *et al,* 2013). Various stimuli can induce or upregulate autophagy. The unc-51 like autophagy activating kinase (ULK)1/ Atg1 complex has been described as the 'mediator of nutrient signalling' regulating the rate of autophagy. The activity of ULK1 is regulated by phosphorylation on specific sites. Adenosine monophosphate-activated protein kinase (AMPK), an energy sensor which responds to low levels of ATP, may phosphorylate ULK1 (at Serine 317 and Serine 777), to promote autophagy, however the phosphorylation of ULK1

(at Serine 757) by mammalian target of rapamycin (mTOR), inhibits autophagy. ULK1 phosphorylates Beclin1 (at Serine 14) to activate the class III phosphatidylinositol 3-kinase (PI3-K) complex, to maintain nutrient and energy homeostasis by balancing the levels of intracellular amino acids, carbohydrates and ATP to the level of autophagy.

Beclin1 (Atg6) is a protein essential for the initial step of phagophore formation and autophagy in general. Beclin1 activity is regulated by binding proteins such as; ambral, ultraviolet radiation resistance associated gene protein (UVRAG) and bif-1 to induce autophagosome formation (Figure 1.3) while proteins such as Bcl-2 and Bcl-XL inhibit autophagy. Beclin1 is the point of cross talk between apoptosis and autophagy, and in response to certain apoptotic stimuli, caspase-3 may also cleave Beclin1. Beclin1s carboxyl-terminal then localizes at the mitochondria to promote apoptosis.
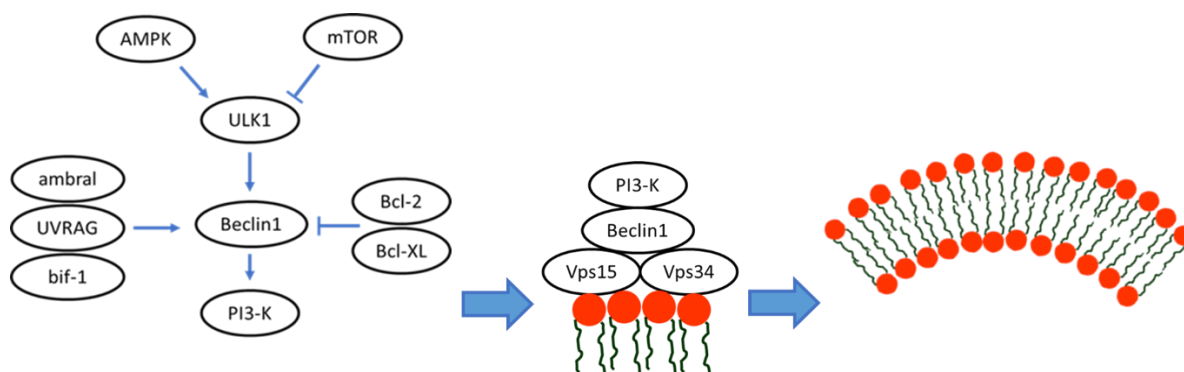
Figure 1.3: Diagram showing the induction of autophagy.

Phagophore formation is the next step of autophagy. The membrane is formed from the cell's phospholipid bilayer. Membrane isolation occurs at the phagophore assembly site (PAS) and is regulated by phosphoinositide 3-kinase (PI3-K) activity. PI3-K exists in a complex with Beclin1, Vps15 and Vps34 (Figure 1.3). After the initial formation, the membranes continue to elongate and sequester intracellular components. In this process; light chain 3 (LC3) is cleaved by Atg4 into LC3-I to expose its carboxyl terminal glycine. LC3-I is converted to LC3-II by Atg7 and Atg3 covalently attaching a phosphatidylethanolamine molecule. A covalently bound Atg5-Atg12-Atg16 complex sequesters LC3-II and lipids for growing the phagophore. Organelles which need to be removed may be targeted by ubiquitin mediated cargo recognition and here, E3 ubiquitin ligases are involved, where the peripheral membrane anchored proteins on the surface of the target organelles are tagged with polyubiquitin molecules. Cytosolic adaptors containing LC3 interaction domains such as p62 and neighbour of BRCA1 gene 1

protein (NBR1) recognize the ubiquitin chains. The LC3 interaction domain can recruit autophagosomes to the target site (Figure 1.4) (Kang *et al,* 2011; Kobayashi, 2015).
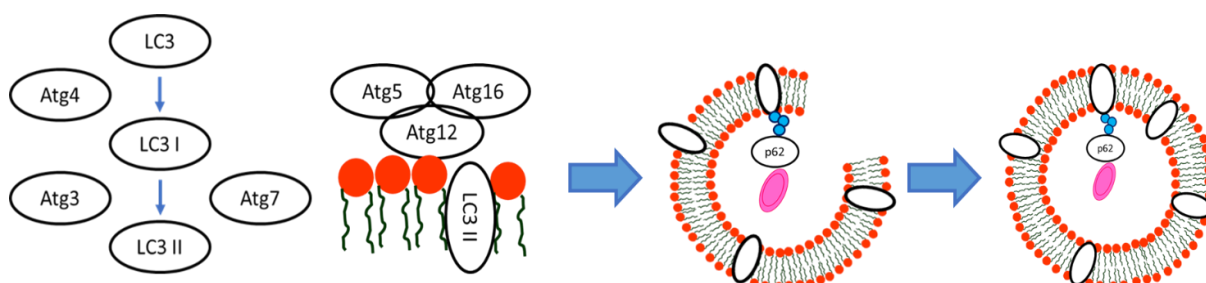
Figure 1.4: Diagram showing the formation of the autophagosome

Once autophagosomes have successfully sequestered their cargo they fuse their membrane with that of the lysosome to have their contents broken down (Figure 1.5) (Kobayashi, 2015; Yang *et al,* 2013).
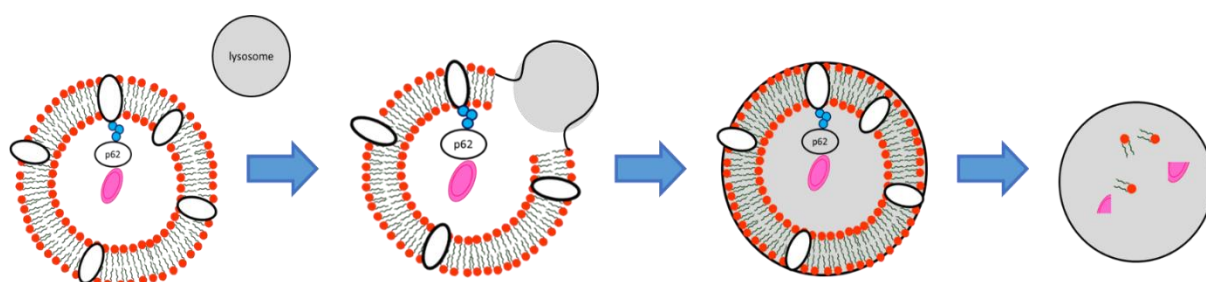
Figure 1.5: Diagram showing autophagolysosomal formation and degradation.

As mitochondria are a site of ATP synthesis, they are very susceptible to oxidative damage. Damaged mitochondria may leak pro-apoptotic proteins into the cytoplasm, inducing a signalling cascade leading to cell death. Damaged and dysfunctional mitochondria are removed through targeted autophagy in a process referred to as mitophagy. During mitophagy, targeted mitochondria are tagged by a ubiquitin ligase such as Parkin, Smurf1, or March5. The ubiquitin tagged mitochondria are recognised by p62 or histone deacetylase 6 (HDAC6) and sent to the autophagosome (Kobayashi, 2015).

1.5.2. Autophagic regulation

During studies which seek to better understand the mechanisms regulating autophagy, the autophagic process has been activated or inhibited at various checkpoints. As autophagic dysregulation is complicit in many diseased states including tumour formation and survival, cardiovascular remodelling and heart failure, activation and inhibition may be key in the treatment of these diseases (Essick & Sam, 2010). Activation (Table 1.2) and inhibition (Table 1.3) of autophagy may be achieved by numerous pharmacological agents (Yang *et al*, 2013).

Table 1.2: List of autophagic activators, Yang *et al*, 2013

Name	Mechanism	Target point
AP23576	mTOR inhibitor	mTOR dependent signalling
Brefeldin A	ER stressing inducer	Autophagy induction
Calpastatin	Calpain inhibitor	mTOR independent signalling
Carbamazepine	IMPase inhibitor	mTOR independent signalling
CCI- 779	mTOR inhibitor	mTOR dependent signalling
Earle's balanced salt solution (EBSS)	Starvation inducer	Autophagy induction
L-690,330	IMPase inhibitor	mTOR independent signalling
Lithium chloride	IMPase inhibitor	mTOR independent signalling
N-Acetyl-D-sphingosine (C2-ceramide)	Class I PI3K inhibitor	mTOR dependent signalling
Penitrem A	Ca2+ channel blocker	mTOR independent signalling
RAD001	mTOR inhibitor	mTOR dependent signalling
Rapamycin	mTOR inhibitor	mTOR dependent signalling
Small molecule enhancers rapamycin (SMER)	mTOR independent activator	mTOR independent signalling
Thapsigargin	ER stressing inducer	Autophagy induction
Trehalose	mTOR independent activator	mTOR independent signalling
Tunicamycin	ER stressing inducer	Autophagy induction
Valproic acid sodium salt	IMPase inhibitor	mTOR independent signalling
Xestospongin B	IP3R blocker	mTOR independent signalling

Table 1.3: List of autophagic inhibitors, Yang *et al,* 2013

Name	Mechanism	Target point
3- Methyladenine	PI 3-kinase inhibitor	Autophagosome formation
Bafilomycin A1	Vacuolar- type H ATPase inhibitor	Autophagolysosome formation
Cycloheximide	Protein sythesis inhibitor	Autophagosome formation
E64d	Acid protease inhibitor	Lysosome
Hydoxycholoroquine	Lysosomal lumen alkalizer	Lysosome
Leupeptin	Acid protease inhibitor	Lysosome
LY294002	PI 3-kinase inhibitor	Autophagosome formation
Lys05	Lysosomal lumen alkalizer	Lysosome
Pepstatin A	Acid protease inhibitor	Lysosome
Wortmaninn	PI 3-kinase inhibitor	Autophagosome formation

1.5.3. Autophagy during cardiac disease

Autophagy occurs in all cells, including cardiac cells, at a basal level under normal conditions and is essential for the turnover of organelles. Upregulation of autophagy has been linked to some cardiac diseases but paradoxically has also been linked to cardioprotection, as upregulation of autophagy may downregulate apoptosis by removing organelles to lower overall nutrient and energy consumption or safely remove damaged mitochondria before they lead to apoptosis (Gustafsson & Gottlieb, 2008).

During cardiac hypertrophy, autophagy appears to be detrimental. Mice which received transverse aortic constriction (TAC) surgery developed hypertrophy as well as an increase in beclin1, LC3-II and other autophagic structures. Myocardial expression of micro ribonucleic acid 30a (miR-30a) was decreased in TAC mouse models and rat heart myoblast (H9c2) cells treated with phenylephrine (PE), an miR-30a inhibitor, increased autophagy as well as the expression of biomarkers of cardiac hypertrophy. Autophagic inhibition however suppressed the cardiomyocyte hypertrophy caused by miR-30a inhibition (Weng *et al*, 2014). Pulmonary arterial hypertension (PAH), a progressive disease linked to cardiac hypertrophy, is characterised by an elevation in pulmonary arterial pressure and right ventricular hypertrophy. Rats were treated with monocrotaline to induce PAH, resulting in an upregulation of autophagy. Autophagic inhibition with chloroquine hindered the development of PAH (Long *et al*, 2013). While the precise mechanisms are unclear it appears that during certain cardiac

hypertrophic pathologies there is an increase in cardiac autophagy and inhibition of this autophagy reduces hypertrophy (Li *et al,* 2016b).

However, during ischemia and reperfusion (I/R), autophagy may limit damage to the myocardium. An increase in the number of autophagosomes correlates to an increase in functional recovery. These autophagosomes often contain mitochondria, which otherwise would have leaked pro-apoptotic proteins into the cell, initiating cell death (Decker & Wildenthal, 1980). An upregulation of autophagy has been linked to a downregulation of apoptosis within the myocardium (Yan *et al,* 2005). Inhibition of autophagy appears to worsen the damage. Mice treated with rapamycin showed a decrease in infarct size whereas mice treated with bafilomycin A1 (BAF- A1), a membrane-permeant lysosomal inhibitor, which inhibits autophagosome-lysosome fusion thus inhibiting the final step of autophagy (degradation), showed an increase in infarct size (Kanamori *et al,* 2011).

Based on the above studies, it is clear that autophagy is a double-edged sword that can be detrimental or beneficial depending on the context in which it is studied.

1.5.4. Autophagy in the context of DOX

There have been numerous studies conducted to evaluate the relationship between DOX treatment and autophagy. Many of these studies have concluded that DOX treatment does affect autophagy. There is however much debate about whether autophagy is upregulated or downregulated in this context. Numerous studies provide evidence for the upregulation of autophagy (Table 4). Rather counterintuitively there are also numerous studies providing evidence for downregulation of autophagy (Table 5). It is worth noting that, although not explicitly stated, majority of these studies appear to be conducted in an acute setting.

The reason for this paradox may be due to many factors. There are many inconsistencies across the studies which may explain the inconsistent results. The choice of model appears to affect the result. Where *in vivo* or *in vitro* studies conducted in rats point to autophagic upregulation, studies conducted in mice point to downregulation. Different studies use different modulators of autophagy. These modulators may have off target effects aside from regulating autophagy which may skew assay results. 3-methyladenine (3-MA) is used to inhibit autophagy in many studies. It has no effect, however, on beclin1-independent forms of autophagy and may upregulate autophagy under certain circumstances. The assays used also differ from study to study as well as the biomarker assessed. Many studies favoured western blots, with the focus

being on LC3 proteins. Many of the earlier studies did not blot for both LC3 and p62 proteins, rather just LC3. Increased LC3 may indicate upregulated of autophagosome formation as this biomarker is present during the early stages of autophagy but this may be incomplete. Studies which blotted for LC3 and p62 showed an increase in both proteins, thus indicating upregulated autophagosome formation but impaired clearance. This means that while autophagy is induced, the cargo is not removed and may lead to detrimental consequences within the cell autophagy (Dirks-naylor, 2013; Klionsky *et al,* 2016; Bartlett *et al,* 2017).

Table 1.4: List of studies suggesting DOX upregulates autophagy

Author, Year	Model	DOX dose	Assay	Treatment
Lu *et al,* 2009	*In vivo*: Male Sprague-Dawley rats *In vitro*: Sprague- Dawley NRCM	*In vivo*: 6x 2.5 mg/kg IP injection (CD: 15 mg/kg) *In vitro*: 1 mg/L -24hrs	WB: Beclin1 FM, FC: Autophagic vacuoles	3-MA
Kobayashi *et al,* 2010	*In vitro*: Sprague- Dawley NRCM	*In vitro*: 1 μM -18 hrs	WB: LC3-II, p62 FM: LC3	3-MA, Rapa, Baf-A1
Chen *et al,* 2011	*In vitro:* Sprague- Dawley NRCM	*In vitro:* 1 μM -16 hrs	WB: LC3-II FM: LC3	3-MA, Rapa, Baf-A1
Dimitrakis *et al,* 2012	*In vitro:* Wistar NRCM	*In vitro:* 1 μM, 10 μM, 20 μM, 50 μM -48hrs	WB: LC3-II FM: LC3	Lactacystin, Chloroquine
Xu *et al,* 2012	*In vitro:* Sprague- Dawley NRCM	*In vitro:* 1μM -18hrs	WB: Beclin1, Atg5, Atg12, LC3-II, p62 FM: LC3	3-MA, Baf-A1, Resveratrol
Smuder *et al,* 2013	*In vivo*: Male Sprague-Dawley rats	*In vivo:* 1x 20 mg/kg IP injection (CD: 20 mg/kg)	WB: Beclin1, Atg5, Atg12, Atg7, Atg4, LC3, Cathepsin	Exercise
Sun *et al,* 2014	*In vivo:* C57BL/6J, ALDH2 KO/ ALDH2 overexpression mouse *In vivo:* NYHA III-IV human tissue In vitro: NMCM, AMCM	*In vivo:* 6x 15 mg/kg IP injection (CD: 90 mg/kg) *In vitro:*1μM -4hrs adult/ 1 μM -18hrs neonatal	WB: Beclin1, Atg5, LC3-II	3-MA, Rapa
Wang *et al,* 2014	*In vivo:* C57BL/6J mouse *In vitro:* H9C2 cells	*In vivo:* 8 mg/kg IP injections (CD: 8 mg/kg) *In vitro:* 10 μM/L -12/24hrs	WB: LC3-II, AMPK, mTOR FM: LC3	3-MA, cpd C, ghrelin
Cao *et al,* 2016	*In vivo:* C57BL/6J mouse *In vitro:* NRCM, H9C2 cells	*In vivo:* 2x 10 mg/kg IP injections (CD: 20 mg/kg) *In vitro:* 0.1-5 μM -24hrs	WB: Beclin1, p62, LC3-I, LC3-II FM: LC3	Rapa, APS

NRCM: Neonatal Rat Cardiomyocytes. NMCM: Neonatal Mouse Cardiomyocytes.
ARCM: Adult Rat Cardiomyocytes. AMCM: Adult Mouse Cardiomyocytes.
IP: Intraperitoneal. CD: Cumulative Dose. WB: Western Blot. FM: Florescence Microscopy. FC: Flow Cytometry.
3-MA: 3-methyladenine. Rapa: Rapamycin. Baf-A1: Bafilomycin-A1.
Cpd C: AMPK inhibitor compound C. APS: Astragalus polysaccharide.

Table 1.5: List of studies suggesting DOX downregulates autophagy

Author, Year	Model	DOX dose	Assay	Treatment
Kawaguchi *et al*, 2012	*In vivo*: GFP-LC3 mouse *In vitro*: GFP-LC3 NMCM	*In vivo:* 2x 10 mg/kg IP injections (CD: 10 mg/kg) *In vitro:* 0.1 µM/L -6hrs	WB: LC3-II, p62 FM: LC3	Chloroquine, Starvation
Hoshino *et al,* 2013	*In vivo:* C57BL/6J, p53/ Parkin/ p21 deficient. GFP- LC3 mouse *In vitro:* HL-1 cardiomyocytes, MEFs	*In vivo:* 5x 2.5mg/kg IP injection (CD: 12.5mg) *In vitro:* 0.02 µM -24hrs	IHC: LC3 EM: autophagic vacuoles	3-MA, Baf-A1
Sishi *et al,* 2013	*In vivo:* GFP-LC3 mouse *In vitro:* H9C2 cells	*In vivo:* 2x 10 mg/kg IP injections (CD: 20 mg/kg) *In vitro:* 3 µM -24hrs	WB: LC3-II, p62	Baf-A1, Rapa
Li *et al,* 2014 (b)	*In vivo:* C57BL/6J, Nrf2−/− mouse *In vitro:* Wistar NRCM	*In vivo*:1x 25 mg/kg IP injection (CD: 25 mg/kg) *In vitro*: 1 µM -24hrs	WB: LC3-II, p62, Atg5, Atg7, Cathepsin	Chloroquine
Katamura *et al,* 2014	*In vivo:* C57BL/6J, GFP-LC3 mouse *In vitro:* Wistar NRCM	*In vivo*:1x 20 mg/kg IP injection (CD: 20mg/kg) *In vitro:* 1 µM -2hrs	WB: LC3-II FM: Autophagic vacuoles	3-MA, Curcumin
Bartlett *et al,* 2016	*In vivo:* Sprague-Dawley rats *In vitro:* NRCM, ARCM, AMCM, H9C2	*In vivo:* 5x 10 mg/kg IP injections (CD:50 mg/kg) *In vitro:*2 µM - 2/6/12/24hrs	WB: ULK1, Beclin1, p62, LC3-I, LC3-II	Chloroquine
Lai *et al,* 2016	*In vivo:* Sprague-Dawley rats *In vitro:* ARCM, H9C2	*In vivo:* 6x 2.5 mg/kg IP injections (CD: 15 mg/kg) *In vitro:* 2 µM	WB: Beclin21, LC3-I, LC3-II	
Li *et al,* 2016 (a)	*In vivo:* Beclin1 +/- mouse *In vitro:* NRCM, H9C2	*In vivo:* 4x 5 mg/kg injections (CD: 20 mg/kg) *In vitro:* 1 µM -24hrs	WB: LC3-1, LC3-II, p62	Baf-A1
Park *et al,* 2016	*In vitro:* human cardiac progenitor cells	*In vitro:* 0.01-5 µM -24hrs	WB: Beclin1, LC3-1, LC3-II, p62 FM: LC3	Rapa
Pizarro *et al,* 2016	*In vitro*: NRCM	*In vitro:* 1 µM -24hrs	WB: Beclin1, LC3-1, LC3-II, p62	3-MA, Rapa, Baf-A1

NRCM: Neonatal Rat Cardiomyocytes. NMCM: Neonatal Mouse Cardiomyocytes.
ARCM: Adult Rat Cardiomyocytes. AMCM: Adult Mouse Cardiomyocytes.
IP: Intraperitoneal. CD: Cumulative Dose. WB: Western Blot. FM: Florescence Microscopy. FC: Flow Cytometry.
3-MA: 3-methyladenine. Rapa: Rapamycin. Baf-A1: Bafilomycin-A1.
Cpd C: AMPK inhibitor compound C. APS: Astragalus polysaccharide.

1.6. Starvation

Starvation is a complex process which affects every system in the body. The literature on starvations effects on these systems is extensive. For the sake of relevance and concision, starvations interactions with autophagy and chemotherapy will only be discussed.

1.6.1. Starvation and autophagy

Starvation is one of the most basic natural inducers of autophagy. During nutrient deprivation, many cell types upregulate autophagy. This may be because organelles no longer receive the nutrients they require to function effectively, or organelles are surplus to cell survival as energy becomes scarce. Biochemically, starvation induces autophagy through AMPK activation of the ULK1/ Atg1 complex (Takeshige *et al*, 1992; Roach, 2011). Cardiomyocytes, like many cell types, upregulate autophagy as a result of starvation. Research conducted by Kanamori *et al* (2009) where mice were starved for 12, 24, 48 and 72 hours, demonstrated a direct correlation between starvation time and autophagic activity. The longer starvation time the greater autophagic activity. It was also observed that under these conditions, ATP levels significantly decreased in the myocardium and autophagy appeared to attenuate this to some extent, as inhibition of autophagy during starvation reduced ATP levels significantly more than starvation alone (when autophagy was allowed to occur). It was concluded that the insufficient ATP supply contributed to the cardiac dysfunction observed in the mice which had autophagy inhibited during starvation. Thus, starvation induced autophagy elicits a cardioprotective effect within this context.

1.6.2. Starvation and chemotherapy

Starvation also elicits protective effects against oxidative stress and chemotherapeutic damage. It was found that in yeasts, worms and mice which were starved prior to oxidative stress induction or etoposide (chemotherapeutic) treatment, the mortality rate was significantly reduced. Although it is unclear why starvation had this protective effect, it is thought that the decrease in IGF1 (caused by starvation) is responsible (Raffaghello *et al,* 2008). While the exact mechanisms remain to be elucidated, there is evidence to suggest that starvation elicits protective effects through multiple pathways, both dependent and independent of autophagy.

More appropriately to this study, starvation prior to DOX treatment elicited a cardioprotective effect. In a study conducted by Kawaguchi *et al* (2012) rats were starved for 48 hrs prior to

DOX treatment. In this study DOX treatment downregulated autophagy, prior starvation however attenuated this downregulation. DOX treatment also depleted myocardial ATP, again autophagy attenuated this. Starvation also improved cardiac function as well as significantly reducing atrophy and fibrosis. This study however was conducted on acute cardiotoxicity.

1.7. Rapamycin

Rapamycin is an mTOR inhibiting drug used to upregulate autophagy. First isolated in the early 1970s from *Streptomyces hygroscopicus* bacteria found in soil on the Easter Islands. It was named rapamycin after the islands native name, Rapa Nui. Originally, rapamycin was shown to have antifungal properties but later shown to have other uses (Vezina *et al,* 1975).

1.7.1. Modes of action

It has since been identified that rapamycin has anti-proliferative and immunosuppressive properties in mammalian cells, thus leading to the investigation of the modes of action of this compound. Rapamycin has previously been shown to be a potent inhibitor of S6K1 activation, a serine/threonine kinase activated by a variety of agonists and an important mediator of PI3-K signalling. Rapamycin forms a functional complex by binding with a 2 kDa FK506-binding protein (FKBP12). This complex binds to and inhibits mTOR complex 1 (mTORC1), a pathway associated with autophagic regulation. Biochemical and genetic analysis of mTOR has shown that two distinct complexes are present; mTOR complex 1 (mTORC1) and mTOR complex 2 (mTORC2). Acute rapamycin exposure only effects (inhibits) mTORC1, however chronic exposure has been shown to inhibit mTORC2 in some cell types (Laplante & Sabatini, 2013). Figure 1.6 shows how rapamycin activates autophagy, compared with starvation. Multiple signals activate mTORC1, including growth factors, nutrients, energy, and oxygen status. Depending on the signal, responses include processes for cell growth and proliferation, micro ribonucleic acid (mRNA) biogenesis, protein, lipid, nucleotide and protein synthesis, energy metabolism, and autophagy. Dysregulation of mTORC1 and the associated pathways are common in cancers. In contrast to mTORC1, far less is known about mTORC2. It has been found that mTORC2 activation of Akt and serum and glucocorticoid-regulated kinase 1 (SGK1) can mediate cell survival (Li *et al,* 2014a).
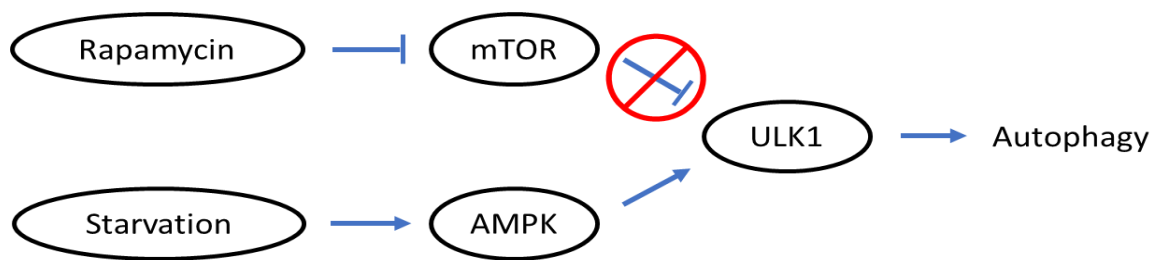
Figure 1.6: Simplified diagram showing starvation vs rapamycin autophagic induction.

1.7.2. Rapamycin and cancers

There are many cancers which display an increase in mTORC1 activation. This is due to either the mutations in oncogenes (Akt, PI3-K, Ras) or tumour suppressors liver kinase B1 (LKB1), phosphatase and tensin homolog (PTEN), tuberous sclerosis proteins 1/2 (TSC1/2) which are upstream regulators of mTORC1. To meet the demands of unregulated proliferation, cancerous cells often possess alterations to energy metabolism and nutrient uptake processes. These processes are directly influenced by the mTORC1 pathways. Oncogenic mTORC1 activation promotes gene expression which is involved in cancer cell metabolic reprogramming. This promotes lipid and protein synthesis, glutamine metabolism and glycolysis (Li *et al,* 2014a).

Due to poor solubility and pharmacokinetics several rapamycin analogs, collectively known as rapalogs, have been developed. Temsirolimus and everolimus, two water-soluble rapalogs, were approved by the Food and Drug Administration (FDA) in 2007 and 2009 respectively, as a treatment for advanced renal cancer carcinoma (RCC). Temsirolimus has been tested in several clinical trials as treatment for advanced or recurrent endometrial cancer, and relapsed or refractory mantle cell lymphoma (MCL) and advanced neuroendocrine carcinoma (NEC) (Benjamin *et al,* 2011). Everolimus was approved by the FDA as a treatment for progressive neuroendocrine tumours (PNET) of pancreatic origin. Trials are also being conducted to evaluate the effect of everolimus as a treatment for advanced gastric cancer, advanced hepatocellular carcinoma and advanced non-small cell lung cancer (NSCLC). Rapalogs have had only modest effects on solid tumours in the clinical setting. The reasons for the modest effects have not been fully established but is likely related to the numerous mTORC1 regulated negative feedback loops supressing upstream signalling, such as PI3-K Akt signalling, receptor tyrosine kinases (RTKs) and Ras-ERK pathways which rapamycin may reactivate. Strategies to overcome these limitations are currently in development (Li *et al,* 2014a).

1.7.3.   Rapamycin and cardioprotection

Rapamycin treatment has a preconditioning-like effect during I/R injury. Mice pre-treated with rapamycin have a significant reduction in infarct size. *In vitro* analysis on cardiomyocytes showed rapamycin reduced apoptosis and necrosis during I/R injury. Cardioprotection may be due to inhibition of protein synthesis and regulation of mitochondrial potassium ATP (mitoKATP) channels. Opening of mitoKATP channels is one method of cardioprotection. It has led to speculation that opening of mitoKATP channels by rapamycin leads to its cardioprotective effect during I/R. The precise mechanism of mitoKATP opening is unclear, there are however some theories. Rapamycin-induced mTOR inhibition upregulates PI3-K and Akt kinases. These kinases are key mediators in the activation of mitoKATP channels. Co-localization of mTOR at the mitochondria allows for the regulation of mitochondrial membrane channel activity (Khan *et al,* 2006). This suggests that rapamycin may be a potentially effective therapy due to its ability to upregulate autophagy, as well as having antineoplastic and cardioprotective effects.

In summation, DOX is an effective and indispensable chemotherapeutic. Cardiotoxicity however is a deadly problem which limits DOX usage. While the mechanisms behind DOX-induced cardiotoxicity are poorly understood it believed to be as a result of increased ROS. Despite this, potential adjuvant therapies like antioxidants and iron chelators which target ROS production, appear to be ineffective or unviable. Despite the contentious literature, it is believed that DOX downregulates autophagy. While the role of autophagy is cardiac disease is poorly understood it has the potential to be an effective adjuvant therapy. Upregulation of autophagy, through pharmacological (rapamycin) or physiological (starvation) inducers, may attenuate the damage by removing damaged cellular components before they can generate deadly signal cascades as well as generate macromolecules to facilitate healing.

1.8. Problem statement

DOX is a potent, effective chemotherapeutic agent that has resulted in an increase in the number of cancer survivors. However due to its severe side effects, especially chronic cardiotoxicity its clinical use is limited. Limited use may have a lesser antineoplastic effect and still may result in cardiotoxicity. This is detrimental to both cancer patients and cancer survivors.

1.9. Hypothesis

DOX treatment reduces autophagic activity which contributes to the detrimental effects observed in the myocardium. Therefore, by upregulating autophagy prior to DOX administration, it is assumed that the negative effects will be attenuated.

1.10.   Aims and objectives

1.10.1. Aims

- To induce an *in vivo* mouse model of prolonged DOX treatment
- Establish DOXs effect on autophagy within this model
- Attenuate cardiotoxicity with rapamycin and starvation

1.10.2. Objectives

- Identify cardiac damage caused by DOX treatment
- Asses levels of autophagic proteins
- Asses the role of oxidative stress and apoptosis in the pathogenesis of cardiotoxicity
- Establish the effects of rapamycin and starvation on DOX induced cardiac damage

Chapter 2: Methodology

2.1. Ethical Considerations and Animal Care

This animal study was reviewed and approved by the Stellenbosch University Animal Ethics committee (reference number: SU-ACUM13-00013). Three-week-old male black 6 mice (C57BL/6) were housed in the animal house at the University of Stellenbosch on a 12-hour day- night cycle and allowed access to food and water *ad libitum*. After one week of acclimatisation, mice were randomly divided into six different treatment groups (Figure 2.1); vehicle (control), DOX, rapamycin, starvation, DOX and rapamycin and DOX and starvation. After an additional week of acclimatisation, the treatment protocol commenced.

2.2. Treatment Protocol
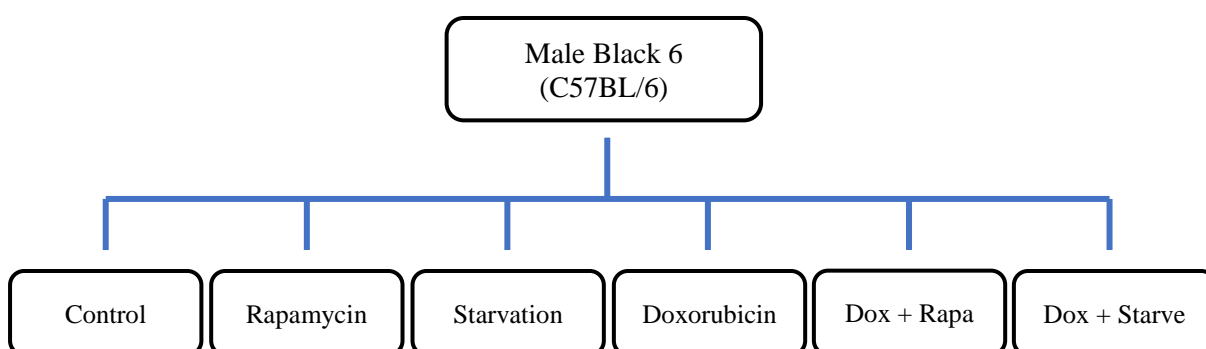
Figure 2.1: Flow Diagram of treatment groups in this study.

The DOX treated group received 2 mg/kg DOX weekly, administered via intraperitoneal injection. This treatment continued for a total of eight weeks, resulting in a cumulative dose of 16 mg/kg. This dosage was found in literature and appears to be amongst the lower dosage range which induces cardiotoxicity, thus mimicking the low dosages given to humans in an attempt to avoid cardiotoxicity. This treatment regimen involves a low dose over an extended period of time rather than a single bolus injection, which results in the gradual development of cardiotoxicity, while reducing other potential acute side effects typically associated with bolus treatment (Bernstein *et al,* 2012; Ghigo *et al,* 2015; Berthiaume *et al,* 2005; Zhou *et al,* 2001).

This treatment regimen also allows multiple pre-treatments, thereby increasing potential cardioprotective effects. The control group (vehicle) received a saline injection of equivocal volume to the DOX treated group. The rapamycin group received 2 mg/kg rapamycin weekly.

This dosage is based on previous research which used rapamycin to induce a cardioprotective effect prior to I/R (Khan *et al,* 2006; Yang *et al,* 2010; Hernández *et al,* 2011). The DOX and rapamycin group received rapamycin 30 minutes prior to receiving DOX.

The starvation group was starved from food for 24 hours each week but were allowed free access to drinking water (Kanamori *et al,* 2009). The DOX and starvation group were starved for 24 hours prior to receiving DOX. These treatment regimens were carried out weekly for a period of eight weeks, and all injections were performed via intraperitoneal injection. Animals were weighed weekly and their welfare was monitored daily. All animals survived the treatment protocol.
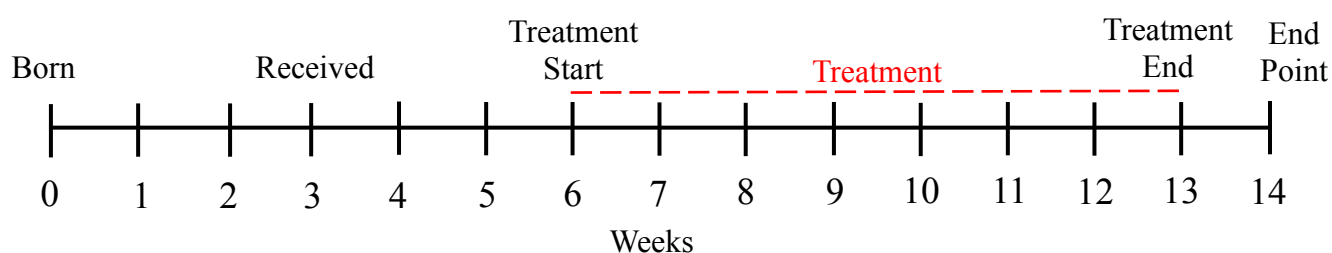
Figure 2.2: Timeline of treatment protocol

2.2.1. Sample collection

One week after the final treatment, mice were euthanised via cervical dislocation. The whole heart was harvested, weighed and sectioned coronally into halves. One half was snap frozen in liquid nitrogen for biochemical analysis and stored at -80 °C. The other half was preserved in a 4% buffered formaldehyde (approximately 10% formalin) solution (Merck, 1004965000) for histological analysis.
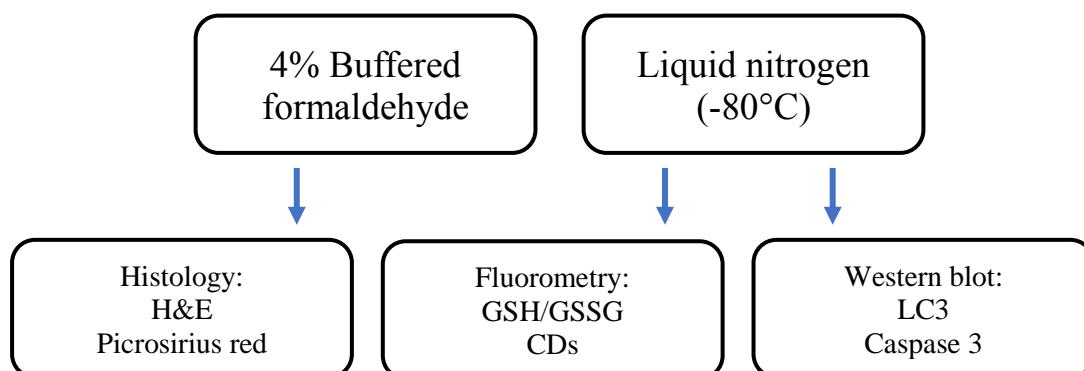
Figure 2.3: Flow Diagram of cardiac samples collected.

2.3. Histological Analysis

2.3.1. Tissue processing

The tissue preserved in buffered formaldehyde solution was processed and embedded in paraffin wax using a Leica EG1150 H tissue processor. After processing, the tissue was sectioned into 5 µm sections using a Leica RM 2125 RT microtome. Cardiac sections were placed in a warm water bath (±40 ℃) then placed onto a glass microscope slide and in a 65 ℃ oven for roughly five minutes to adhere (full protocol available in Appendix B, page 59).

2.3.2. Haematoxylin & Eosin (H&E) stain

H&E staining was performed in order to assess the general morphology of the tissue and to measure the cross-sectional area of the cardiomyocytes. The cationic haematoxylin stains the negatively charged substances within the tissue (such as DNA) blue and the anionic eosin stains the positively charged substances within the tissue (such as proteins) pink. This stain was performed using a Leica ST5010 Autostainer XL automated staining machine (full protocol available in Appendix B, page 60).

2.3.3. Picrosirius red stain

The Picrosirius red stain was performed in order to assess the amount of fibrosis within the tissue. The hydrophilic Sirius red binding to acid groups on the collagen fibres while the hydrophobic picric acid staining the rest of the tissue yellow. This stain was performed by hand (full protocol available in Appendix B, page 60).

2.3.4. Image analysis

The stains were imaged using a Nikon Eclipse E4000 microscope and NIS Elements imaging software (version 4.10) and analysed using ImageJ software (version 1.49). The H&E images were captured at 40x magnification and stitched together to create an image of the entire organ section. These images were used to assess any major structural abnormalities. In a modification of the imaging protocol used by Gilliam *et al* (2009), 6 random H&E images were taken per treatment group, at 200x magnification and 10 fibres were measured per image.

In modification of the imaging protocol used by Kanamori *et al* (2011), 15 random picrosirius red images were taken per group, at 400x magnification. Fibrosis was displayed as a percentage of the total tissue area.

2.4. Biochemical analysis

2.4.1. Oxidative Stress analysis

Fluorometry was conducted to assess oxidative stress levels. Glutathione (GSH), glutathione disulfide (GSSG) and conjugated dienes (CDs) levels were assessed. GSH levels were compared to GSSG, the oxidized form of GSH, as a ratio. This provided an assessment of ROS and as GSSG is reduced back to GSH, an assessment of antioxidant status as well. CDs act as a marker of early lipid peroxidation and thus are indicative of oxidative damage in general (John Betteridge, 2000; Zitka *et al,* 2012).

For the GSH assay tissue was homogenised in phosphate buffer and for the GSSG assay tissue was homogenised in a 1% 1-Methyl-2-vinylpyridinium triflate phosphate (M2VP) buffer solution. The homogenates were centrifuged at 12 000 rpm, the pellet was discarded, and the supernatant was used. Absorbance was measured at 412 nm every 30 seconds for three minutes using a Fluoroskan Ascent Microplate Fluorometer (Thermo Fisher Scientific), GraphPad Prism (version 6.01) was used to generate a standard curve. The concentrations of total GSH and GSSG were then calculated using the standard curve of GSH (full protocol available in Appendix B, page 63).

To perform the CDs assay, excess lysate from the GSH group was modified. A 1:2 ratio of chloroform: methanol was added to the lysates. The lysates were centrifuged at 14 000 rpm. The bottom layer in the heterogeneous solution was removed and refrigerated overnight to allow evaporation. The next day, cyclohexane was added, and the lysates were analysed by measuring the absorbance at 380 nm. Concentration was calculated by dividing the absorbance by the excitation coefficient (full protocol available in Appendix B, page 64).

2.4.2. Western blot analysis

Western blots were performed to assess apoptotic and autophagic levels through the protein expression of caspase 3 (apoptotic marker) and LC3 (autophagic marker), respectively. Tissue lysates were prepared by homogenizing tissue in radioimmunoprecipitation assay (RIPA) buffer. The homogenates were centrifuged at 15 000 rpm, the pellet was discarded, and the supernatant was centrifuged again. A Direct Detect Spectrometer was used to calculate the total protein concentration. This method of protein quantification involves pipetting a small amount of the protein lysate onto a hydrophilic polytetrafluoroethylene (PTFE) membrane. Mid-Infrared (MIR) light is then used on the membrane, allowing for amide detection and subsequent protein quantification. Protein samples were prepared in Laemmli's buffer and 20 µg of protein was loaded in each well. Proteins were separated on a 12% acrylamide gel run at 100V for approximately three hours. The proteins were transferred to a low-fluorescence polyvinylidene fluoride (LF PVDF) membrane using a Trans-Blot Turbo Transfer System ready-to-assemble (RTA) Transfer kit (Bio-Rad, 170 - 4274). The membranes were blocked in 5% milk for two hours then incubated in primary antibody solution (1:1000) for approximately 72 hours at 4 °C under constant agitation. The membranes were then washed in tris buffered saline with tween 20 (TBS-T) and incubated in the appropriate secondary antibody (1:1000) for one hour at room temperature under constant agitation. Enhanced chemiluminescent (ECL) detection was used to image membranes, clarity ECL substrate (Bio-Rad, 170 - 5061) was added and membranes were imaged on a ChemiDoc XRS+ system (Bio-Rad, 170 - 8265) (full protocol available in Appendix B, page 66).

Table 2.1: List of Antibodies used.

Primary antibodies			
Name	Size (kDa)	Company	Catalogue no
Caspase 3	35	Cell Signalling	9665
LC-3	16,14	Cell Signalling	2775
Secondary antibody			
Name		Company	Catalogue no
Anti- mouse IgG, HRP-linked Antibody		Cell Signalling	7076

2.5. Statistical analysis

Due to sample size a Kolmogorov- Smirnov (KS) normality test was done to test for a normal distribution of data. If distribution was normal, an analysis of variance (ANOVA) was conducted to test for significant differences across the groups. A Fisher's Least Significant Difference (LSD) post hoc test was applied, where appropriate, as it mimics the t-test. If distribution was non-normal, a Kruskal-Wallis test was conducted to test for significant differences across groups. A t-test was done to compare specific groups if the groups were both normally distributed, if however, one (or both) were non-normally distributed a Mann-Whitney U test was done. All values are presented as mean ± standard error of mean (SEM). Statistical analyses were conducted in GraphPad Prism (version 6.01). P-values were considered significant when $P < 0.05$.
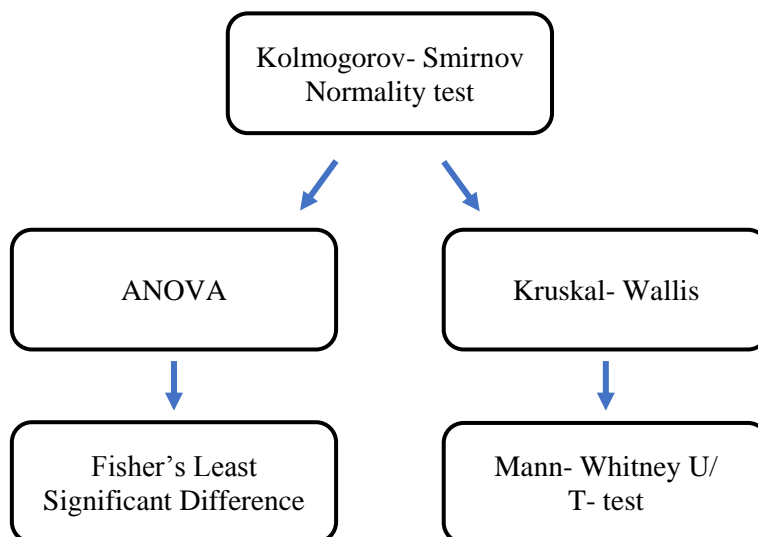
Figure 2.4: Flow Diagram of statistical tests used

Chapter 3: Results

3.1. Physical assessment

3.1.1. Animal mass

As DOX treatment is known to induce weight loss, the experimental animals in this study were weighed weekly to determine the effect of DOX on animal mass. Furthermore, as some of the animals were starved in order to induced autophagic activity, either in the presence or absence of DOX, it was important to monitor these animals for any changes in weight. Animals were initially weighed at week one, prior to any treatment. Treatment began at week two and ended at week nine. Animals were then euthanised at week 10. Significant differences were observed between the control and all the DOX groups (Figure 3.1). These differences were first observed in week five and continued until the end of the study.
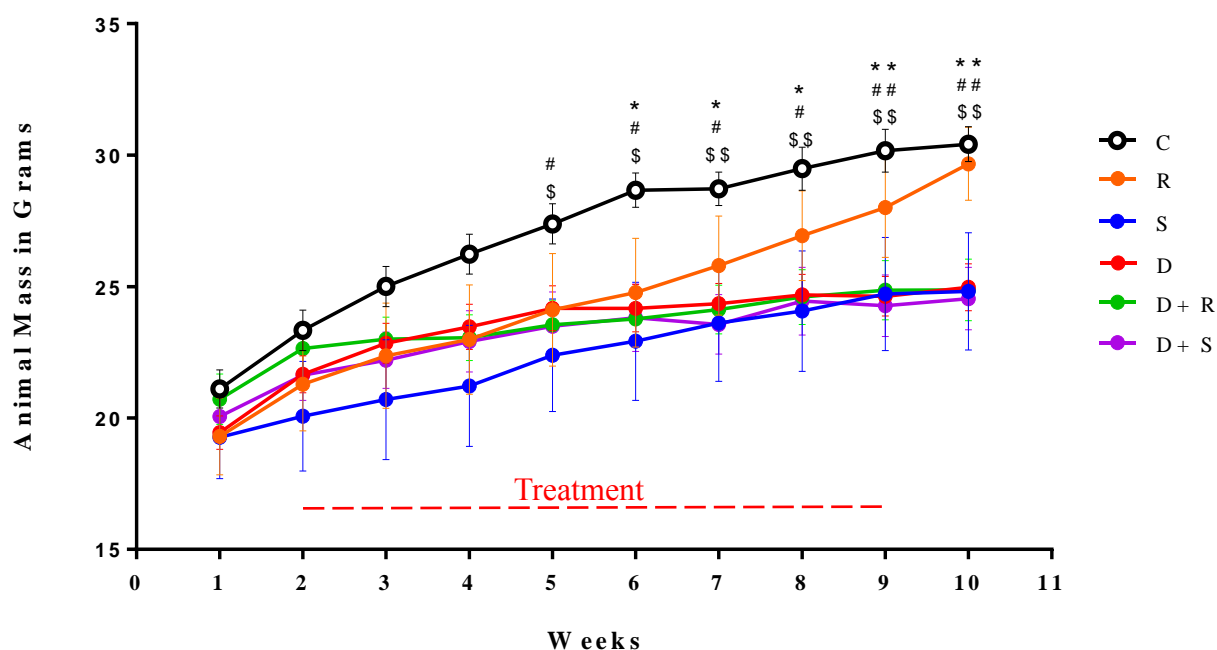
Figure 3.1: Line graph displaying animal mass in grams over time in weeks. Red line indicating treatment duration. DOX vs Control (*), DOX+ Rapa vs Control (#) and DOX+ starve vs Control ($). Single symbol (p<0.05), Double symbol (p<0.01). All data displayed in g as mean ± SEM. n=6-7. Abbreviation: C (control), R (rapamycin), S (starvation), D (DOX), D+R (DOX+ Rapa), D+S (DOX+ Starve)

3.1.2. Cardiac mass

To determine the effect of DOX and the adjuvant therapies on myocardial mass, the wet weight of the organ was taken following euthanasia. The mass of the heart was then compared to the mass of animal. This was done to assess potential hypertrophy or atrophy of cardiac muscle. No significant differences were present (Table 3.1).

Table 3.1: Cardiac mass in mg and cardiac mass as a ratio to animal body weight, displayed in arbitrary units. All data displayed as mean± SEM. n=6-7.

	Control	Rapamycin	Starvation	DOX	DOX + Rapa	DOX + Starve
Cardiac mass (mg)	184.50± 25.28	168.30± 19.91	127.50± 17.93	160.90± 14.43	143.70± 12.31	144.70± 14.56
Cardiac: Animal mass (AU)	6.013± 0.699	5.937± 0.470	5.077± 0.350	6.410± 0.462	5.804± 0.470	5.864± 0.439

3.2. Histological analysis

3.2.1. Overall qualitative assessment

As previously mentioned, DOX treatment causes cardiac damage. Whole heart images showed microscopic damage, to some degree, across all groups. However due to poor image quality it is not possible to infer whether the damage seen in the groups occurred as a result of the treatment protocol or post mortem during the tissue processing and staining procedures (Figure 3.3).

3.2.2. Cardiomyocyte area

DOX treatment is known to cause cardiomyocyte death and negatively affect cardiac function. Measurement of cardiomyocyte cross-sectional area or 'thickness' is a good assessment of cardiac health, as these cells are responsible for the contractions of the heart. Therefore, a loss of cardiomyocytes or a decrease in cardiomyocyte area may correlate to a decrease in cardiac function. A significant decrease in cardiomyocyte area was observed in the DOX group (97.41 ± 4.1, $p<0.01$) compared to the control group (112.6 ± 4.32). There are significant differences between other groups, but none relevant to this study.
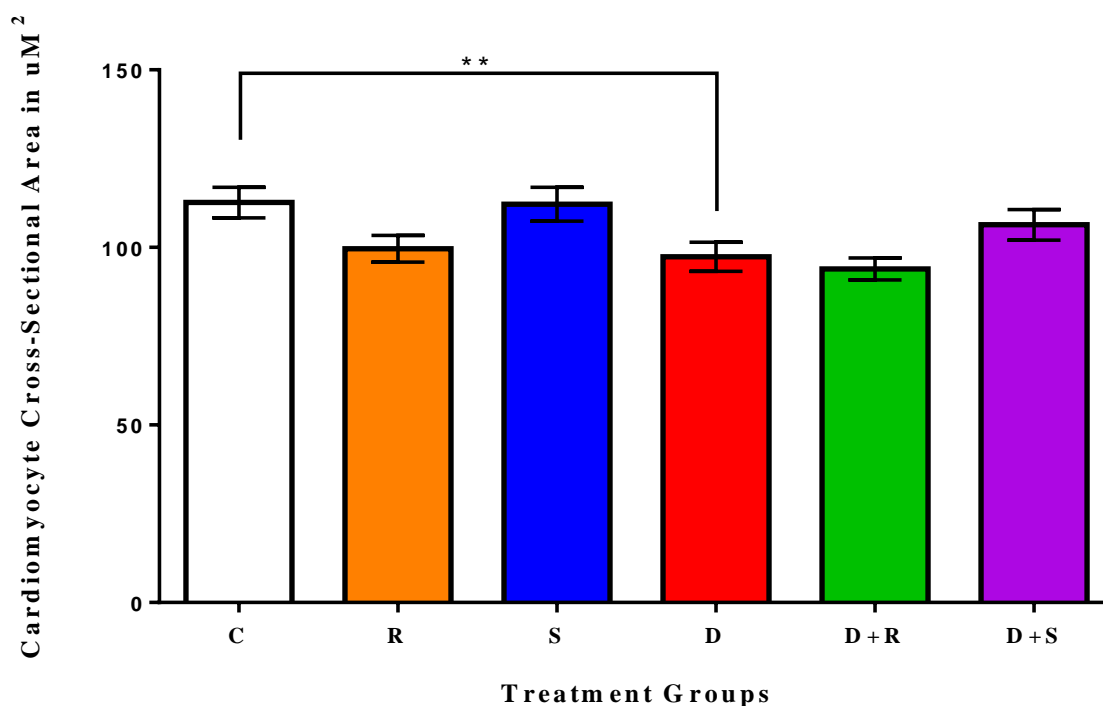
Figure 3.2: Average Area of Cardiac Cardiomyocytes in um^2. Values expressed as mean ± SEM (**$p<0.01$), (n=6) Abbreviation: C (control), R (rapamycin), S (starvation), D (DOX), D+R (DOX+ Rapa), D+S (DOX+ Starve)
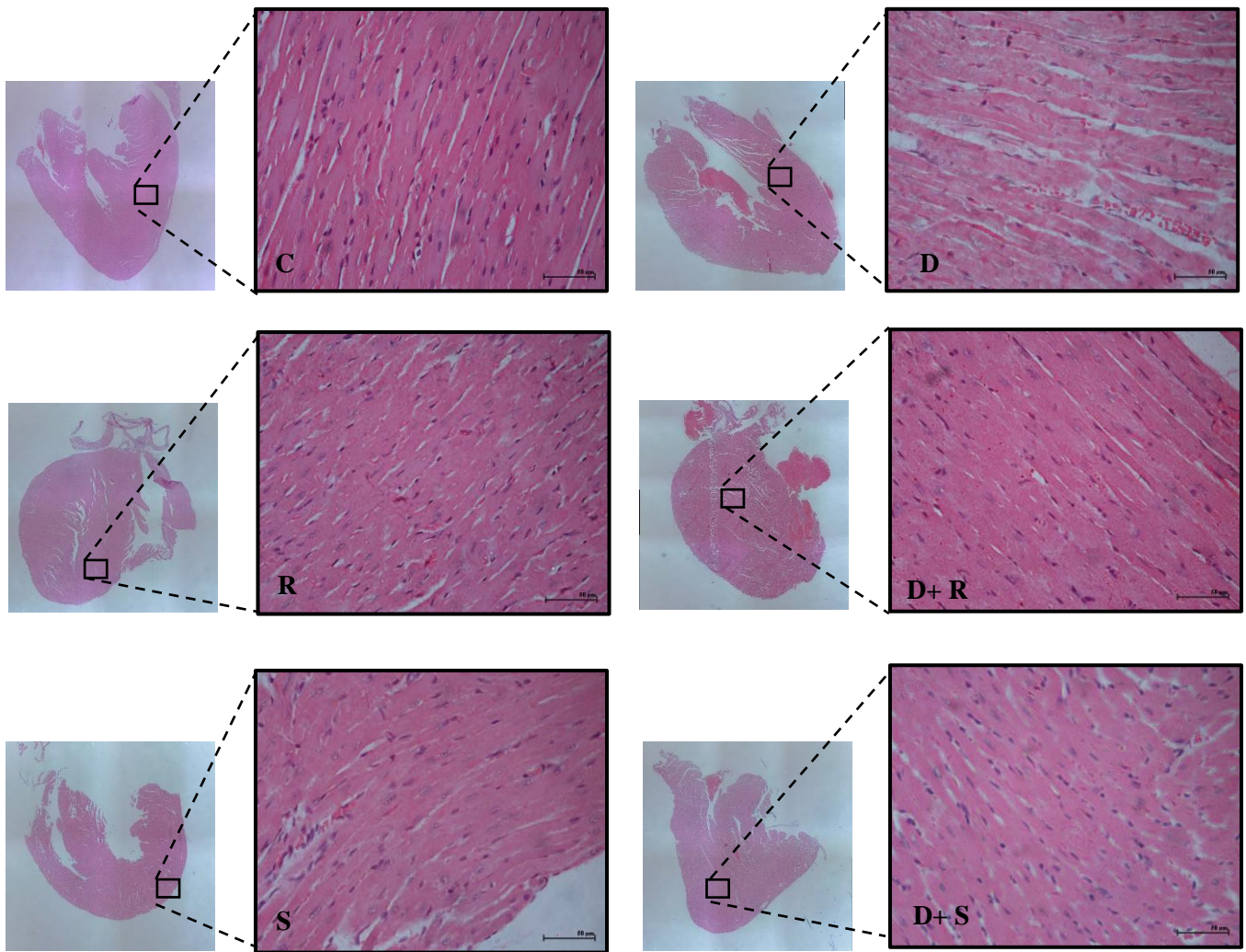
Figure 3.3: Haematoxylin and Eosin stained cardiac tissue. Whole images expanded to 400x magnification. Scale bar = 50µm. Abbreviation: C (control), R (rapamycin), S (starvation), D (DOX), D+R (DOX+ Rapa), D+S (DOX+ Starve)

3.2.3. Fibrosis

The extracellular matrix (ECM) of the heart is comprised of fibrous connective tissue. During certain stresses fibroblast proliferation is upregulated and thus many cardiac pathologies, including DOX exposure, result in excessive fibrous tissue in the ECM. Measuring the amount of fibrous tissue in the heart is a good indicator of cardiac health as excessive fibrosis may decrease cardiac function. A significant increase in fibrosis was observed in the DOX group (2.07± 0.22, p<0.001) compared to the control group (1.05± 0.18). There was also a significant decrease in fibrosis in the DOX+ starve group (1.21± 0.18, p<0.01) compared to the DOX group (2.07± 0.22) (Figure 3.5). There are significant differences between other groups, but none relevant to this study.
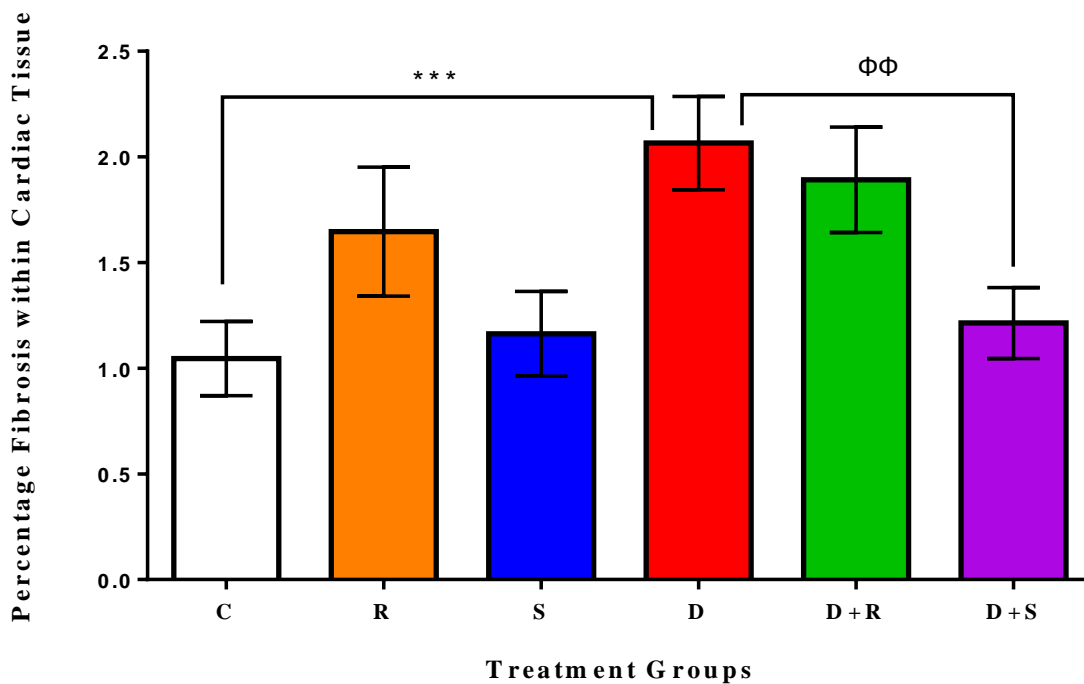
Figure 3.4: Average Percentage of Cardiac fibrosis. Values expressed as mean ± SEM (***p<0.001), (ΦΦp<0.01), (n=3) Abbreviation: C (control), R (rapamycin), S (starvation), D (DOX), D+R (DOX+ Rapa), D+S (DOX+ Starve)
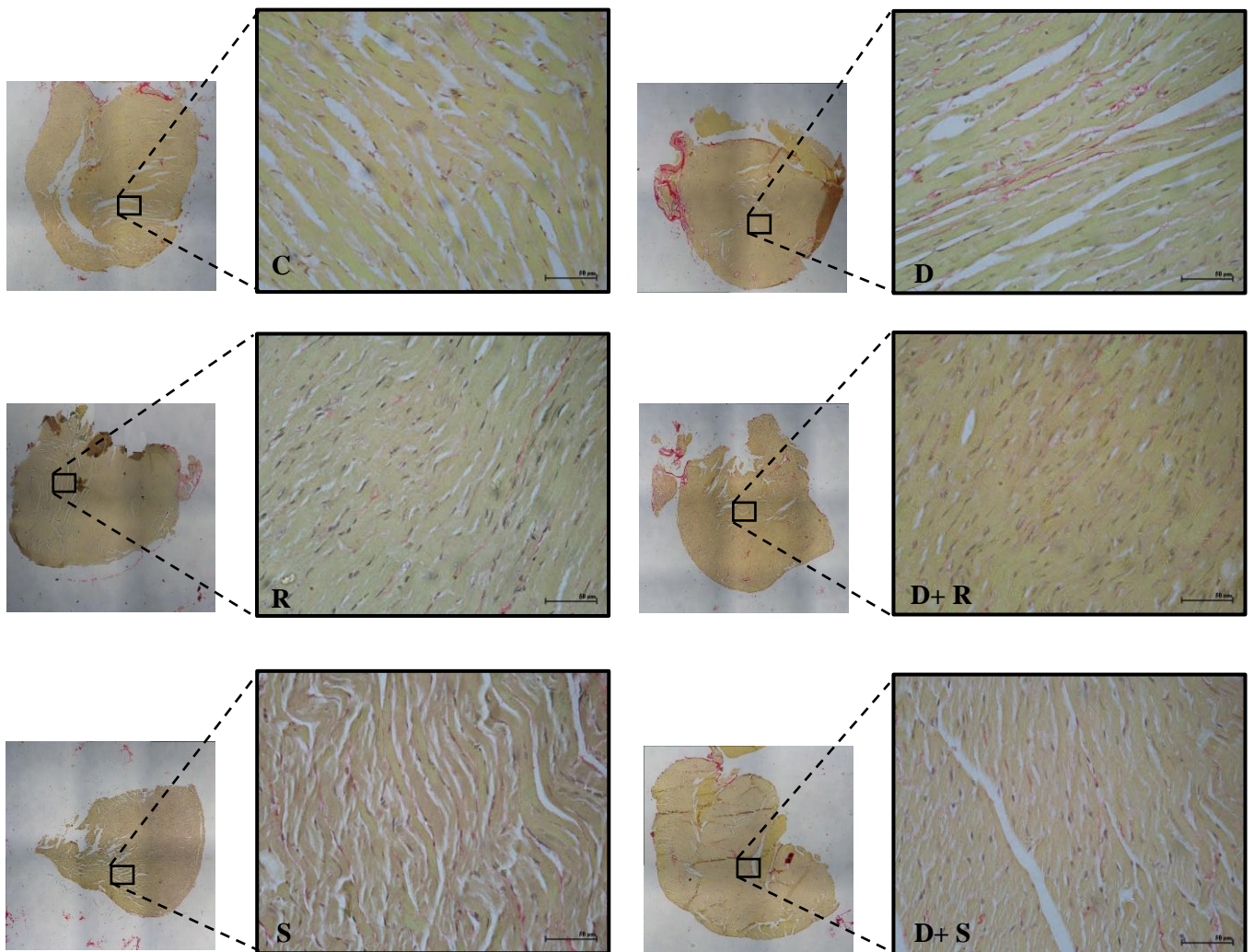
Figure 3.5: Picrosirius red stained cardiac tissue. Whole images expanded to 400x magnification. Red indicating fibrious tissue. Yellow indicating non- fibrious tissue. Scale bar = 50µm. Abbreviation: C (control), R (rapamycin), S (starvation), D (DOX), D+R (DOX+ Rapa), D+S (DOX+ Starve)

3.3. Oxidative Stress Markers

It is often proposed that the most likely mechanism of action for DOX-induced cardiotoxicity is oxidative stress. Because of this the effects of DOX, and the adjuvant therapies, on oxidative stress levels were measured.

3.3.1. Antioxidant Status

When GSH neutralizes free radicals it donates an electron, oxidizing to GSSG. Therefore, a decrease in GSH coupled with an increase in GSSG is indicative of a state of oxidative stress. Both GSH and GSSG were measured and a ratio of GSH: GSSG was used as a marker of oxidative stress. The GSH: GSSG ratio was analysed. No significant differences were present.

Table 3.2: GSH and GSSG in µMol/g and GSH: GSSG ratio in arbitrary units as mean± SEM. n=3-6.

	Control	Rapamycin	Starvation	DOX	DOX + Rapa	DOX + Starve
GSH (µMol/g)	0.4429± 0.0548	0.4004± 0.0631	0.3725± 0.0857	0.4447± 0.0126	0.4023± 0.0479	0.4221± 0.0607
GSSG (µMol/g)	0.0344± 0.0051	0.0380± 0.0032	0.0415± 0.0017	0.0413± 0.0014	0.0373± 0.0013	0.0397± 0.0015
GSH: GSSG (AU)	0.0879± 0.0228	0.1202± 0.0417	0.1278± 0.0356	0.0932± 0.0040	0.0966± 0.0107	0.1040± 0.0178

3.3.2. Lipid peroxidation

Unsaturated fatty acids found in cell (and other organelle) membranes are a common target for free radicals. This oxidation results in a CDs. CDs are an early marker of lipid peroxidation as they may undergo further oxidation to form other products. No significant differences were present.

Table 3.3: CDs expressed in µMol/g as mean± SEM. n=4-6.

	Control	Rapamycin	Starvation	DOX	DOX + Rapa	DOX + Starve
CDs (µMol/g)	0.0585± 0.0064	0.0498± 0.0036	0.0567± 0.0056	0.0883± 0.0247	0.0694± 0.0093	0.0787± 0.0048

3.4. Western blot

3.4.1. Apoptosis

Caspase 3 is an executioner caspase, it is responsible for cleaving various proteins within the cell causing DNA damage and eventually successful apoptosis. Caspase 3 exists in 2 forms, the inactive procaspase (35 kDa) and the cleaved active caspase (17/19 kDa). Protein levels were measured against stain-free total protein instead of β-actin or glyceraldehyde 3-phosphate dehydrogenase (GAPDH), as it is believed to produce more accurate results (Gilda & Gomes 2013). The whole inactive protein was detected but the cleaved active protein was not. No significant differences were present.
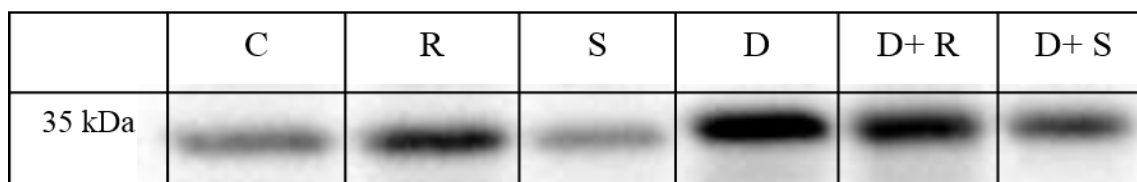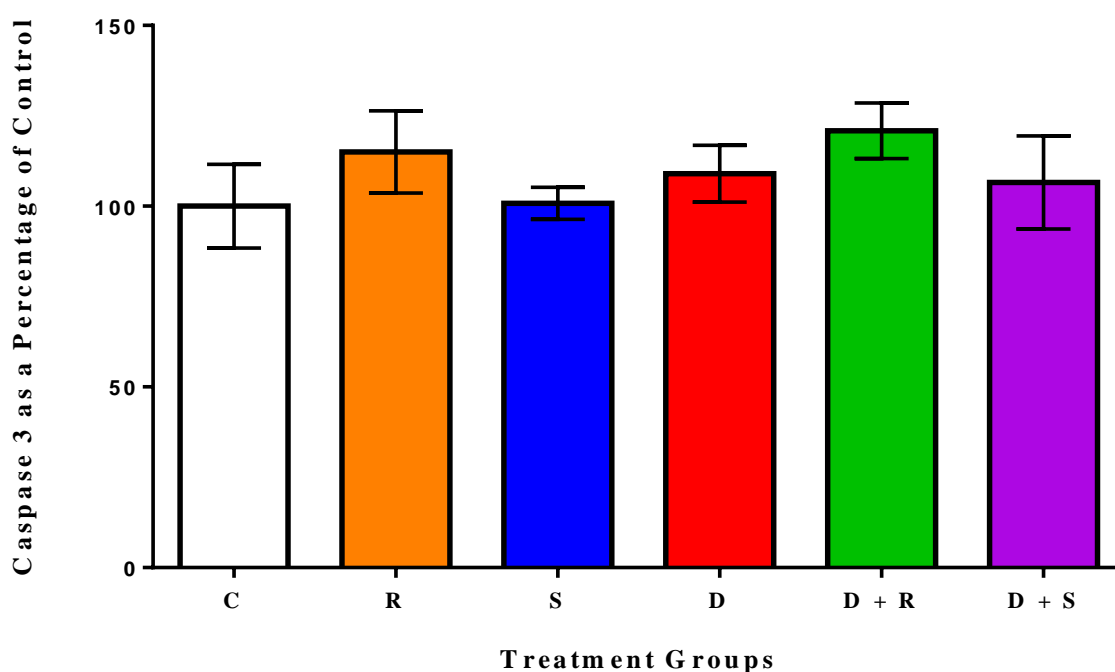
Figure 3.6: Caspase 3 protein expression. Values expressed as a percentage of control as mean ± SEM. n=4-6. Representative western blot bands for each group. Abbreviation: C (control), R (rapamycin), S (starvation), D (DOX), D+R (DOX+ Rapa), D+S (DOX+ Starve)

3.4.2. Autophagy

During the formation of autophagic vacuoles, LC3-I (14 kDa) is converted to LC3-II (16 kDa). Both LC3-I and LC3-II were measured and a ratio of LC3-II: LC3-I was used as a marker autophagy. Protein levels were measured against stain-free total protein. The LC3-II: LC3-I ratio was analysed. A significant decrease in autophagy was observed in the DOX group (0.3733± 0.0683, p> 0.01) compared to the control group (1.1420± 0.2262). There was also a decrease in the DOX+ Rapa (0.4344± 0.0543, p> 0.05) and DOX+ starve (0.4818± 0.1240, p> 0.05) compared to the control group. There are significant differences between groups, but none relevant to this study.
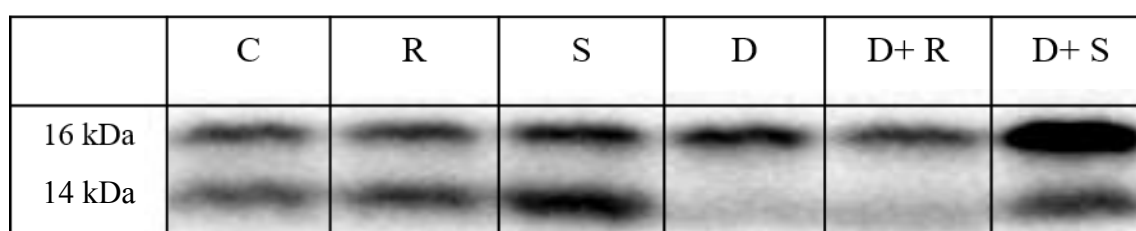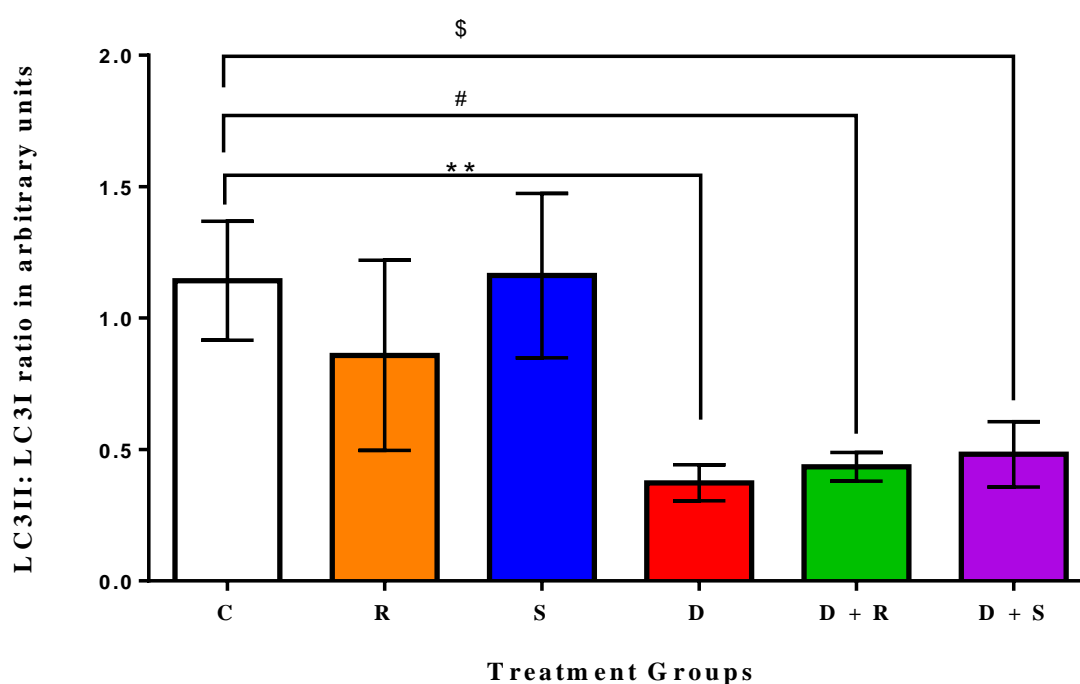
Figure 3.7: LC3 protein expression. Values expressed in arbitrary units as mean ± SEM. (**p<0.01), ($^\#$p<0.05), ($^\$$p<0.05), (n=3-5). Representative western blot bands for each group. Abbreviation: C (control), R (rapamycin), S (starvation), D (DOX), D+R (DOX+ Rapa), D+S (DOX+ Starve)

Chapter 4: Discussion and Conclusion

This study investigated a potential treatment for attenuating the harmful effects associated with DOX administration *in vivo*. As previously mentioned, chronic cardiotoxicity is dose-dependent, irreversible and linked with an unfavourable outcomes for affected patients. Moreover, when this condition ensues, the affected patients are no longer on chemotherapy and thus begs the question: what happens from the time a patient completes chemotherapy to the time when the cardiovascular complications becomes evident? Based on this question it is clear to see how difficult, if not impossible, it is to simulate this condition in pre-clinical models.

Due to the complexity and life-threatening nature of the chronic form of cardiotoxicity, not only is it necessary to understand the molecular mechanisms involved, it is also necessary to identify potential adjuvant therapies. While cell culture experiments are simple to execute, they do not effectively mimic what is observed in cancer survivors; and it is for this reason that it is necessary to establish clinically relevant animal models. An interesting observation made in the literature is that the majority of *in vivo* studies published to date have utilized supra-physiological concentrations of DOX in the acute setting and thus caution should be made when interpreting the results. Herman & Ferrans (1998) indicated that the use of smaller doses of DOX administered over an extended period of time in animals is more clinically relevant, and better simulates the myocardial alterations associated with chronic cardiotoxicity. The cumulative dose (total dose used for duration of study) used by the above indicated authors was 15 mg/kg for rats, administered over a couple of weeks. However, in mouse models (Table 1.4 and Table 1.5), cumulative doses range from 12.5 – 90 mg/kg. Guided by the above information, a cumulative dose of 16 mg/kg DOX (2 mg/kg over eight weeks) was administered to mice in this study due to the fact that it is amongst the lower dosage range which induces cardiotoxicity, and therefore mimics the low dosages given to humans in an attempt to avoid cardiotoxicity. Furthermore, this concentration falls within the clinical range of 60 - 75 mg/m^2 that is administered to humans (human equivalent dose) (Desai *et al*, 2013).

Autophagic activity in the heart has long being viewed as paradoxical; either being beneficial in one context and detrimental in another, all of which depends on the type (Matsui *et al*, 2007) and duration (Kang *et al*, 2008; Loos *et al*, 2011) of the stress, injury, and levels of autophagic activity (Eisenberg-Lerner *et al*, 2009) at the time. Considering that autophagy is additionally complemented by other forms of cell death such as apoptosis, it is challenging to ascertain whether it is pro-survival or pro-death. As such, this cross-talk between autophagy and

apoptosis has since been differentiated into three categories, namely: autophagy and apoptosis can stimulate cell death synergistically, or autophagy can promote survival by inhibiting apoptosis, or autophagy can allow apoptosis to occur alone without death caused by autophagy (Eisenberg-Lerner *et al*, 2009).

This study has demonstrated that DOX treatment significantly downregulated autophagic activity when compared to the control (Figure 3.7). Although the exact mechanism by which DOX inhibits autophagy is yet to be discovered, other studies have suggested that DOX inhibits AMPK and ULK1 activity (autophagy promoters), and increases mTOR activity (autophagy inhibitor) (Kawaguchi *et al*, 2012; Park *et al*, 2016). While our results agree with the literature, it is important to note that the duration, dose, frequency of treatment, as well as the model simulated in this study is different in many aspects to that observed in the literature (Table 1.4 and Table 1.5). This studies pre-treatment protocol, with either rapamycin or starvation, did not appear to attenuate autophagic downregulation in the DOX combination groups. This may be due to a number of reasons. Firstly, since rapamycin was administered to the experimental animals 30 minutes prior to DOX, this may not have been sufficient time to upregulate autophagy maximally to counteract the potent inhibitory actions of DOX on autophagy. Furthermore, since the half-life of rapamycin is indicated to be $58 - 63$ hours (Nalbandian *et al*, 2015) and that of DOX is 17.7 hours in rodents (Rahman *et al*, 1986), the timing of the termination of the study did influence the results obtained as both the effects of the drugs at the time of termination have declined. Secondly, starvation, a potent mechanism used to stimulate autophagy, was induced 24 hours prior to DOX. Once DOX was administered, the animals were free to access food *ad libitum*. This return of nutrients thus returned autophagy to basal levels, however due the presence of DOX, the inhibitory action of this chemotherapeutic agent took over. Thirdly, since this study was terminated a week after the last injections and by this time the animals had access to food, the levels of autophagy detected in this study are only reflective of the levels of autophagy at that point in time.

Myocardial apoptosis and oxidative stress are commonly cited characteristics of DOX-induced cardiotoxicity (Kumar *et al*, 2001; Kobayashi *et al*, 2010). This observation is supported by others (Shan *et al*, 1996; Kang *et al*, 2001; Arola *et al*, 2000) who have implicated the involvement of both the intrinsic and extrinsic apoptotic pathways of apoptosis and elevated oxidative stress levels after DOX treatment. This study however did not definitively demonstrate apoptosis induction (Figure 3.6) or changes in the oxidative stress parameters analysed (Table 3.2 and Table 3.3). This was rather surprising considering the overwhelming

amount of literature available regarding their roles in this context. In the presence of ROS, GSH is oxidized to GSSG, changing the ratio of GSH to GSSG. Even though this imbalance may be indicative of oxidative stress, this change is time-dependent as GSSG is eventually reduced back to GSH. The time of sample collection thus becomes an important factor when evaluating changes in glutathione. Similar to our results, Deng *et al* (2015) showed no changes in glutathione levels 72 hours after a single 15 mg/kg bolus administration of DOX despite other markers of oxidative damage being evident. Interestingly, Zhang *et al* (2015) illustrated significant changes in the GSH:GSSG ratio 48 hours but not after two weeks following weekly DOX doses of 2 mg/kg over five weeks.

In contrast to the GSH:GSSG ratio which measures oxidative stress indirectly by evaluating the anti-oxidant status, CDs are markers of lipid peroxidation which is indicative of oxidative damage. Lipid peroxidation is the result of ROS removing a hydrogen atom from a fatty acid chain (usually polyunsaturated fatty acids), generating unpaired electrons. The fatty acid undergoes rearrangement which results in two double bonds being separated by a single bond, i.e. a conjugated diene (John Betteridge, 2000). It is not uncommon to detect no significant changes in CDs even if lipid peroxidation has occurred. CDs are formed in the early stages of lipid peroxidation and in time will undergo further changes. Malondialdehyde (MDA) is the end product of the peroxidative decomposition of polyunsaturated fatty acids and is thus considered a late marker of lipid peroxidation. In the context of DOX toxicity, Nowak *et al* (1995) demonstrated peak CD levels in the heart after 24 hours compared to MDA levels that peaked after 48 hours. A similar observation was made by Murin *et al* (2001) where CD levels peaked between 2 - 24 hours and declined by 48 hours, while MDA levels remained elevated throughout these time points in an ischemia/reperfusion model. Together, these studies suggest that while elevated levels of ROS may have occurred, a state of oxidative stress induced, ultimately resulting in oxidative damage. The ratio of GSG:GSSG and CD analysis may not be the most sensitive indicators of oxidative stress after 48 hours of an intervention as redox homeostasis is restored. The above may also explain why no changes in apoptotic activity was observed in this study considering that apoptosis is triggered as a direct consequence to DOX-induced oxidative stress.

Oxidative stress and inflammation cannot be easily separated as both conditions can influence one another. Inflammation which leads to fibrosis is an additional factor known to contribute to DOX-induced cardiotoxicity. Usually, fibrosis encompasses homeostasis, inflammation, proliferation and finally remodelling (Diegelmann & Evans, 2004). In the course of

homeostasis and inflammation, macrophages and neutrophils are recruited by particular cytokines to the injury site where they activate resident fibroblasts. Through the proliferation of these fibroblasts, they deposit collagen which occupies and replaces apoptotic cardiomyocytes (Khan & Sheppard, 2006). The tissue damage that occurs and the resulting inflammation that ensues increases ROS, which in turn enhances the release of fibrotic factors. Fibrosis is thus an important component of the repair process; however its accumulation can result in organ dysfunction, and eventually failure over time. This study noted significant fibrosis in the DOX group and significantly less fibrosis in the group that was starved prior to DOX administration (Figure 3.4), suggesting a potentially protective effect of starvation, despite the lack of autophagic attenuation. The histological changes associated with DOX treatment in this study not only consisted of fibrosis, but also a loss of cardiomyocyte area (Figure 3.2) as indicated by Šimůnek *et al* (2004). The reduction is cardiomyocyte area in the DOX treated group is indicative of protein degradation via the ubiquitin proteasome pathway (UPP), a major proteolytic pathway responsible for intracellular protein degradation (Gruene *et al*, 2004), since autophagy in this group was downregulated. Ubiquitination refers to the process of conjugation between free ubiquitin (Ub) and a substrate protein. Ub, a highly conserved molecule ubiquitously expressed in all eukaryotes, covalently attaches to targeted proteins in linear chains involving three enzymes: Ub-activating enzymes (E1), Ub-conjugating enzymes (E2) and Ub-ligases (E3) which recognize a specific substrate and thus transfers the activated Ub molecule to a lysine residue of that specific substrate (Willis & Patterson, 2006; Patterson *et al*, 2007; Powell, 2006). Substrates marked in a poly-ubiquitin manner at lysine 48, results in the substrate being targeted for proteasomal degradation. In catabolic states where proteolysis is prominent, specific E3 ligases, Muscle Ring Finger-1 (MuRF-1) and atrogin1/MAFbx (Muscle Atrophy F-box) are upregulated in a forkhead box (FoxO)-dependent manner (Bodine *et al*, 2001), and therefore regulate the ubiquitination of cardiomyocyte proteins for subsequent degradation (de Palma *et al*, 2008). However, the observed reduction in cardiomyocyte area in the DOX group did not impact on the overall myocardial weight (Table 3.1).

It is possible that the induction of proteasomal specific ubiquitination contributed to the overall weight loss observed (Figure 3.1). It may also be a result of differences in food consumed (Table A1, Appendix A). It was not possible to statistically asses if there were differences in amount of food consumed so this too is just speculation. Further research is however required to confirm either of these statements in this model of prolonged DOX treatment.

In conclusion, the present study investigated the therapeutic potential of elevated autophagy using a pharmacological (rapamycin) and a physiological (starvation) approach, in an attempt to reduce the cardiac side effects associated with DOX treatment. Although the model utilized is unique and displayed some characteristics of DOX cardiotoxicity; mainly physical (body weight) and structural (cardiomyocyte area and cardiac fibrosis), the biochemical characteristics (oxidative stress and apoptosis) measured produced inconclusive results. These results may imply that biochemical changes are transient or that structural modifications take place before biochemical changes occur. Therefore, no definitive conclusions can be drawn on the precise effects and mechanisms of action of these therapeutic intervention within this scenario and further investigation is necessary.

Limitations and Future Recommendations

Like other studies, this study has its limitations and can be improved on going forward. While numerous limitations and future recommendations can be made, only a few will be listed, focused on and discussed.

Greater sample size

A major limitation of this model was the relatively small sample size (n = 6-7 per group). As each animal is unique, their responses to the same stimuli differs, and thus creates variability in the data collected. A larger sample size attenuates this variability allowing for greater statistical accuracy. A greater sample size would also be an advantage in this study due to the choice of rodent model utilized and the number of experiments performed. A mouse heart is much smaller than a rat heart, and in this case, some experiments were performed with a sample size of n = 3-4 per group.

Additional time points

Considering that the majority of data collected in this study was taken at the end of the treatment protocol and the experiments performed reflected this time point, it is likely that the early changes induced by DOX and/or autophagy upregulation may have been missed. Therefore, by adding earlier time points in to this study, we would be able to determine the

extent of biochemical alterations and whether they lead to structural modifications over the duration of the treatment protocol.

Evaluation of cardiac function

A decline in cardiac function (particularly LVEF), changes in heart rate and blood pressure, and abnormal ECG alterations are all signs of DOX toxicity. Due to the lack of cardiac function data, the model of DOX-induced cardiotoxicity was not fully validated. Further studies should thus include measurements of cardiovascular function either through echocardiography, working heart or Langendorff perfusions; and cardiovascular markers of damage such as cardiac troponins.

Other considerations

The measuring of inflammatory markers (e.g.: c-reactive protein and pro-inflammatory cytokines) to complement the fibrotic data and asses the inflammatory state of disease.

The measuring of markers of autophagy (e.g.: p62, AMPK, mTOR) and apoptosis (e.g.: cleaved poly adenosine diphosphate-ribose polymerase (PARP), cytochrome c) would add value to this study as these would be able to indicate whether our intervention was sufficient to elevate autophagy.

Multiple measurements of antioxidant activity, oxidative damage and oxidative status to fully understand the level of oxidative stress in myocardium across the different groups. Bearing in mind the timing of sample collection.

A group with an autophagic inhibitor should be included to act as a negative control. This will allow for a more comprehensive assessment of the role of autophagy in this context.

43

References

Adlam, V. J., Harrison, J. C., Porteous, C. M., James, A. M., Smith, R. A. J., Murphy, M. P., & Sammut, I. A. (2017). Targeting an Antioxidant to Mitochondria Decreases Cardiac Ischemia-Reperfusion Injury. *The Federation of American Societies for Experimental Biology*, 19(9), 1088–1095.

Arcamone, F., Cassinelli, G., Fantani, G., Grein, A., Orenzzi, P., Pol, C., & Spalla, C. (1969). Adriamycin, 14-Hydroxydaunomycin, a New Antitumor Antibiotic from S. peucetius var. caesius. *Biotechnology and Bioengineering*, 11(6), 1101–1110.

Arola O.J., Saraste A., Pulkki K., Kallajoi M., Parvinen M., & Voipio-Pulkki L.M. (2000). Acute Doxorubicin Cardiotoxicity Involves Cardiomyocyte Apoptosis. *Cancer Research*, 60(17), 89–92.

Ashford, T. P., & Porter, K. R. (1962). Cytoplasmic Components in the Hepatic Cell Lysosomes. *Journal of Cell Biology*, 12(1), 198–202.

Bartlett, J. J., Trivedi, P. C., & Pulinilkunnil, T. (2017). Autophagic Dysregulation in Doxorubicin Cardiomyopathy. *Journal of Molecular and Cellular Cardiology*, 104, 1–8.

Bartlett, J. J, Trivedi, P. C., Yeung, P., Kienesberger, P. C., & Pulinilkunnil, T. (2016). Doxorubicin Impairs Cardiomyocyte Viability by Suppressing Transcription Factor EB Expression and Disrupting Autophagy. *Biochemical Journal*, 473, 3769–3789.

Benjamin, D., Colombi, M., Moroni, C., & Hall, M. N. (2011). Rapamycin Passes the Torch: A New Generation of mTOR Inhibitors. *Nature Reviews*, 10(November), 868–880.

Bernstein, D., Fajardo, G., & Zhao, M. (2012). The Role of β-adrenergic Receptors in Heart Failure: Differential Regulation of Cardiotoxicity and Cardioprotection. *Progress in Paediatric Cardiology,* 31(1), 35–38.

Berthiaume, J. M., Oliveira, P. J., Fariss, M. W., & Wallace, K. B. (2005). Dietary Vitamin E Decreases Doxorubicin-induced Oxidative Stress Without Preventing Mitochondrial Dysfunction. *Cardiovascular Toxicology*, 5(3), 257–267.

Bodine, S. C., Stitt, T. N, Gonzalez, M., Kline, W. O., Stover, G. L., Bauerlein, R., Zlotchenko, E., Scrimgeour, A., Lawrence, J. C., Glass, D. J., Yancopoulos, G. D. (2001). Akt/mTOR

Pathway is a Crucial Regulator of Skeletal Muscle Hypertrophy and can Prevent Muscle Atrophy in vivo. *Nature Cell Biology*, 3(11), 1014-1009.

Bristow, M. R., Thompson, P. D., Martin, R. P., Mason, J. W., & Billingham, M. E. (1978). Early Anthracycline Cardiotoxicity. *The American Journal of Medicine*, 65(November), 823–832.

Cao, Y., Shen, T., Huang, X., Lin, Y., Chen, B., & Pang, J. (2016). Astragalus Polysaccharide Restores Autophagic Flux and Improves Cardiomyocyte Function in Doxorubicin-induced Cardiotoxicity. *Oncotarget*, 8(3), 4837–4848.

Chen, K., Xu, X., Kobayashi, S., Timm, D, Jepperson, T., & Liang, Q. (2011). Caloric Restriction Mimetic 2-Deoxyglucose Antagonizes Doxorubicin-induced Cardiomyocyte Death by Multiple Mechanisms. *The Journal of Biological Chemistry*, 286(25), 21993–22006.

Cutts, S., Nudelman, A., Rephaeli, A., & Phillips, D. (2005). The Power and Potential of Doxorubicin-DNA Adducts. *International Union of Biochemistry and Molecular Biology Life*, 57(2), 73–81.

De Palma, L., Marinelli, M., Pavan, M., Orazi, A., (2008). Ubiquitin ligases MuRF1 and MAFbx in Human Skeletal Muscle Atrophy. *Joint Bone Spine* 75, 53–57.

Decker, R. S., & Wildenthal, K. (1980). Lysosomal Alterations in Hypoxic and Reoxygenated Hearts. *American Journal of Pathology*, (98), 425–444.

Deng, J., Coy, D., Zhang, W., Sunkara, M., Morris, A. J., Wang, C., & Jungsuwadee, P. (2015). Elevated Glutathione Is Not Sufficient to Protect against Doxorubicin-Induced Nuclear Damage in Heart in Multidrug Resistance − Associated Protein 1 (Mrp1 / Abcc1) Null Mice. *The Journal of Pharmacology and Experimental Therapeutics*, 355, 272–279.

Desai, V.G., Herman, E.H., Moland, C.L., Branham, W.S., Lewis, S.M., Davis, K.J., George, N.I., Lee, T., Kerr, S. & Fuscoe, J.C. (2013). Development of Doxorubicin-induced Chronic Cardiotoxicity in the B6C3F1 Mouse Model. *Toxicology and Applied Pharmacology*, 266 (1), 109–121.

Diegelmann, R. & Evans, M. (2004). Wound Healing: An Overview of Acute, Fibrotic and Delayed Healing. *Frontiers in Bioscience*, 9, 283–289.

Dimitrakis, P., Timolati, F., & Suter, T. M. (2012). Effects of Doxorubicin Cancer Therapy on Autophagy and The Ubiquitin-Proteasome System in Long-term Cultured Adult Rat Cardiomyocytes. *Cell and Tissue Research*, 350, 361–372.

Dirks-Naylor, A. J. (2013). The Role of Autophagy in Doxorubicin-induced Cardiotoxicity. *Life Sciences,* 93(24), 913–916.

Eisenberg-Lerner, A., Bialik, S., Simon, H.U., Kimchi, A. (2009). Life and Death Partners: Apoptosis, Autophagy and Cross-Talk Between Them. *Cell Death and Differentiation*, 16(9), 66–75

Elmore, S. (2007). Apoptosis: A Review of Programmed Cell Death. *Toxicologic Pathology,* 35(4), 495–516.

Essick, E. E., & Sam, F. (2010). Oxidative Stress and Autophagy in Cardiac Disease, Neurological Disorders, Aging and Cancer. *Oxidative Medicine and Cellular Longevity*, 3(3), 168–177.

Florescu, M., Cintenza, M., & Vinereanu, D. (2013). Chemotherapy-induced Cardiotoxicity. *Maedica - A Journal of Clinical Medicine*, 8(1), 59–67.

Frishman, W. H., Sung, H. M., Yee, H. C., Liu, L. L., Keefe, D. L., Einzing, A. I., & Dutcher, J. P. (1996). Cardiovascular Toxicity with Cancer Chemotherapy. *Current Problem in Cardiology*, 21(4), 227–286.

Gewirtz, D. A. (1999). A Critical Evaluation of the Mechanisms of Action Proposed for the Antitumor Effects of the Anthracycline Antibiotics Adriamycin and Daunorubicin. *Biochemical Pharmacology*, 57(7), 727–741.

Ghigo, A., Li, M., & Hirsch, E. (2015). New Signal Transduction Paradigms in Anthracycline-induced Cardiotoxicity. *Biochimica et Biophysica Acta - Molecular Cell Research*, 1863(2016), 1916–1925.

Gilda, J. E., & Gomes, A. V. (2013). Stain-Free Total Protein Staining is a Superior Loading Control to b -actin for Western Blots. *Analytical Biochemistry*, 440(2), 186–188.

Gilliam, L., Ferreira, L.F., Bruton, J.D., Moylan, J.S., Westerblad, H., St Clair, D.K. & Reid, M.B. (2009). Doxorubicin acts through tumor necrosis factor receptor subtype 1 to cause dysfunction of murine skeletal muscle. *Journal of Applied Physiology*. 107 (6), 1935–1942.

Glick, D., Barth, S., & Macleod, K. F. (2010). Autophagy: Cellular and Molecular Mechanisms. *Journal of Pathology*, 211, 3–12.

Goodman, M. F., Bessman, M. J., & Bachurt, N. R. (1974). Adriamycin and Daunorubicin Inhibition of Mutant T4 DNA Polymerases. *Proceedings of the National Academy of Sciences of the United States of America*, 71(4), 1193–1196.

Goormaghtigh, E., Chatelain, P., Caspers, J., Ruysschaert, J. M., & Triomphe, B. (1980). Evidence of a Complex Between Adriamycin Derivatives and Cardiolipin: Possible Role in Cardiotoxicity. *Biochemical Pharmacology,* 29, 3003–3010.

Gruene, T., Jung, T., Merker, K., Davies, K.J. (2004). Decreased Proteolysis Caused by Protein Aggregates, Inclusion Bodies, Plaques, Lipofuscin, Ceroid, and Aggresomes During Oxidative Stress Aging, and Disease. *International Journal of Biochemistry & Cell Biology*. 36, 2519–2530.

Gustafsson, A. B., & Gottlieb, R. A. (2008). Recycle or Die: The Role of Autophagy in Cardioprotection. *Journal of Molecular and Cellular Cardiology*, 44(4), 654–661.

Herman, E. H., & Ferrans, V. J. (1998). Animal Models of Anthracycline Cardiotoxicity: Basic Mechanisms and Cardioprotective Activity. *Progress in Paediatric Cardiology*, 8, 49–58.

Hernández, G., Hind, L., Fidalgo, M., Guerrero, A., Zalvide, J., Force, T., & Pombo, C. M. (2011). A Novel Cardioprotective p38-MAPK/mTOR Pathway. *Experimental Cell Research*, 4(164), 2938–2949

Hoshino, A., Mita, Y., Okawa, Y., Ariyoshi, M., Iwai-kanai, E., Ueyama, T., & Matoba, S. (2013). Cytosolic p53 Inhibits Parkin-mediated Mitophagy and Promotes Mitochondrial Dysfunction in the Mouse Heart. *Nature Communications*, 4(2308), 1–12.

Ichikawa, Y., Ghanefar, M., Bayeva, M., Wu, R., Khechaduri, A., Naga Prasad, S. V., & Ardehali, H. (2014). Cardiotoxicity of Doxorubicin is Mediated Through Mitochondrial Iron Accumulation. *Journal of Clinical Investigation*, 124(2), 617–630.

John Betteridge, D. (2000). What Is Oxidative Stress? *Metabolism*, 49(2), 3–8.

Kanamori, H., Takemura, G., Goto, K., Maruyama, R., Tsujimoto, A., Ogino, A., & Minatoguchi, S. (2011). The Role of Autophagy Emerging in Postinfarction Cardiac Remodelling. *Cardiovascular Research*, 91, 330–339.

Kanamori, H., Takemura, G., Marauyama, R., Goto, K., Tsujimoto, A., Takeyama, T., & Minatoguchi, S. (2009). Functional Significance and Morphological Characterization of Starvation-Induced Autophagy in the Adult Heart. *The American Journal of Pathology*, 174(5), 1705–1714.

Kang, C., & Avery, L. (2008). To Be or Not To Be, The Level of Autophagy is The Question: Dual Roles of Autophagy in The Survival Response to Starvation. *Autophagy*, 4.

Kang, Y. J. Molecular and Cellular Mechanisms of Cardiotoxicity. (2001). *Environmental Health Perspectives*, 109, 27–34.

Kang, R., Zeh, H. J., Lotze, M. T., & Tang, D. (2011). The Beclin 1 Network Regulates Autophagy and Apoptosis. *Cell Death and Differentiation*, 18(4), 571–80.

Katamura, M., Iwai-kanai, E., Nakaoka, M., Okawa, Y., Ariyoshi, M., Mita, Y., & Ikeda, K. (2014). Curcumin Attenuates Doxorubicin-Induced Cardiotoxicity by Inducing Autophagy via the Regulation of JNK Phosphorylation. *Journal of Clinical and Experimental Cardiology*, 5(9), 1–8.

Kawaguchi, T., Takemura, G., Kanamori, H., Takeyama, T., Watanabe, T., Morishita, K., & Minatoguchi, S. (2012). Prior Starvation Mitigates Acute Doxorubicin Cardiotoxicity Through Restoration of Autophagy in Affected Cardiomyocytes. *Cardiovascular Research*, 96, 456–465.

Keizer, H. G., Pinedo, H. M., Schuurhuis, G. J., & Joenje, H. (1990). Doxorubicin (Adriamycin): A Critical Review of Free Radical-Dependent Mechanisms of Cytotoxicity. *Pharmacology and Therapeutics*, 47, 219–231.

Kerr, J., Wyllie, A., & Currie, A. (1972). Apoptosis: A Basic Biological Phenomenon with Wide-Ranging Implications in Tissue Kinetics. *British Journal of Cancer*, 239(26), 239– 257.

Khan, R., & Sheppard, R. (2006). Fibrosis in Heart Disease: Understanding the Role of Transforming Growth Factor-b 1 in Cardiomyopathy, Valvular Disease and Arrhythmia. *Immunology*, 118, 10–24.

Khan, S. A., Salloum, F., Das, A., Xi, L. W., Vetrovec, G. C., & Kukreja, R. (2006). Rapamycin Confers Preconditioning-like Protection Against Ischemia-reperfusion Injury in Isolated Mouse Heart and Cardiomyocytes. *Journal of Molecular and Cellular Cardiology*, 41(2), 256–264.

Klionsky, D. J., Abdelmohsen, K., Abe, A., Abedin, J., Abeliovich, H., Arozena, A. A., & Besteiro, S. (2016). Guidelines for the Use and Interpretation of Assays for Monitoring Autophagy (3rd edition). *Autophagy*, 12(1), 1–222.

Kobayashi, S. (2015). Cell Death in Neuromuscular Diseases Choose Delicately and Reuse Adequately: The Newly Revealed Process of Autophagy. *Biological and Pharmaceutical Bulletin*, 38(8), 1098–1103.

Kobayashi, S., Volden, P., Timm, D., Mao, K.., Xu, X, & Liang, Q. (2010). Transcription Factor GATA4 Inhibits Doxorubicin-induced Autophagy and Cardiomyocyte Death. *The Journal of Biological Chemistry*, 285(1), 793–804.

Kumar, D., Kirshenbaum, I. A., Li, T., Danelisen, I., & Singal, P. K. (2001). Apoptosis in Adriamycin Cardiomyopathy and it's Modulation by Probucol. *Antioxidant and Redox Signal*, 3, 135–45.

Lai, L., Chen, J., Wang, N., Zhu, G.., Duan, X, & Ling, F. (2016). MiRNA-30e Mediated Cardioprotection of ACE2 in Rats with Doxorubicin-induced Heart Failure Through Inhibiting Cardiomyocyte Autophagy. *Life Sciences*, 169, 69–75.

Langer, S. W. (2014). Dexrazoxane for the Treatment of Chemotherapy-related Side Effects. *Cancer Management and Research*, 6, 357–363.

Laplante, M., & Sabatini, D. M. (2013). mTOR Signaling in Growth Control and Disease. *Cell*, 149(2), 274–293

Lefrak, E. A., Pitha, J., Rosenheim, S., & Gottlieb, J. A. (1973). A Clinicopathologic Analysis of Adriamycin Cardiotoxicity. *Cancer*, 32(2), 302–314.

Li, D. L., Wang, Z. V., Ding, G., Tan, W., Luo, X., Criollo, A., Hill, J. A. (2016) (a). Doxorubicin Blocks Cardiomyocyte Autophagic Flux by Inhibiting Lysosome Acidification. *Circulation*, 113, 1668–1687.

Li, J., Kim, S. G., & Blenis, J. (2014) (a). Rapamycin: One Drug, Many Effects. *Cell Metabolism*, 19(3), 373–379.

Li, L., Xu, J., He, L., Peng, L., Zhong, Q., Chen, L., & Jiang, Z. (2016) (b). The Role of Autophagy in Cardiac Hypertrophy. *Acta Biochimica et Biophysica Sinica*, 48(6), 491–500.

Li, S., Wang, W., Niu, T., Wang, H., Li, B., Shao, L., Cui, T. (2014) (b). Nrf2 Deficiency Exaggerates Doxorubicin-Induced Cardiotoxicity and Cardiac Dysfunction. *Oxidative Medicine and Cellular Longevity*, 2014, 1–15.

Long, L., Yang, X., Southwood, M., Lu, J., Marciniak, S. J., Dunmore, B. J., & Morrell, N. W. (2013). Chloroquine Prevents Progression of Experimental Pulmonary Hypertension via Inhibition of Autophagy and Degradation. *Circulation Research*, 1159–1170.

Loos, B., Lochner, A., & Engelbrecht, A. M. (2011) Autophagy in Heart Disease: A Strong Hypothesis for an Untouched Metabolic Reserve. *Medical Hypotheses*, 77, 52–7.

Lu, L., Wu, W., Yan, J., Li, X., Yu, H., & Yu, X. (2009). Adriamycin-induced Autophagic Cardiomyocyte Death Plays a Pathogenic Role in a Rat Model of Heart Failure. *International Journal of Cardiology*, 134(1), 82–90.

Marty, M., Espie, M., Llombart, A., Monnier, A., Rapoport, B. L., & Stahalova, V. (2006). Multicenter Randomized Phase III Study of the Cardioprotective Effect of Dexrazoxane (Cardioxane) in Advanced/ Metastatic Breast Cancer Patients Treated with Anthracycline-based Chemotherapy. *Annals of Oncology*, 17(4), 614–622.

Matsui, Y., Takagi, H., Qu, X., Abdellatif, M., Sakoda, H., & Asano, T. (2007) Distinct Roles of Autophagy in the Heart During Ischemia and Reperfusion: Roles of AMP Activated Protein Kinase and Beclin 1 in Mediating autophagy. *Circulation Research*, 100, 914–22.

Minotti, G., Menna, P., Salvatorelli, E., Cairo, G., & Gianni, L. (2004). Anthracyclines: Molecular Advances and Pharmacologic Developments in Antitumor Activity and Cardiotoxicity. *Pharmacological Reviews*, 56(2), 185–229.

Muggia, F. M., & Green, M. D. (1991). New Anthracycline Antitumor Antibiotics. *Critical Reviews in Oncology and Hematology*, 11(1), 43–64.

Muindi, J. R. F., Sinha, B. K., Gianni, L., & Myers, C. E. (1984). Hydroxyl Radical Production and DNA Damage Induced by Anthracyclin Iron complex. *Federation of European Biochemical Societies*, 172(2), 226–230.

Murin, R., Drgrova, A., Kaplan, P., Dobrota, D., & Lehotsky, J. (2001). Ischemia/ Reperfusion-induced Oxidative Stress Causes Structural Changes of Brain Membrane Proteins and Lipids. *General Physiology and Biophysics*, 20, 431–438.

Murphy, M. P., & Smith, R. A. J. (2000). Drug Delivery to Mitochondria: The Key to Mitochondrial Medicine. *Advanced Drug Delivery Reviews*, 41, 235–250.

Myung, S. K., Ju, W., Cho, B., Oh, S.W., Park, S. M., Koo, B. K., & Park, B. J. (2013). Efficacy of Vitamin and Antioxidant Supplements in Prevention of Cardiovascular Disease: Systematic Review and Meta-analysis of Randomised Controlled. *British Medical Journal*, 10, 1–22.

Nalbandian, A., Llewellyn, K. J., Nguyen, C, Yazdi, P. G., & Kimonis, V. E. (2015). Rapamycin and chloroquine: The in vitro and in vivo Effects of Autophagy- Modifying Drugs Show Promising Results in Valosin Containing Protein Multisystem Proteinopathy. *Public Library of Science*, 10, 1–16

Nitiss, J. L. (2009). DNA Topoisomerase II and its Growing Repertoire of Biological Functions. *Cancer*, 9, 327–337.

Nowak, D., Pierscinski, G., & Drzewoski, J. (1995). Ambroxol Inhibits Doxorubicin- Induced Lipid Peroxidation in Heart of Mice. *Free Radical Biology and Medicine*, 19(5), 659–663.

Octavia, Y., Tocchetti, C. G., Gabrielson, K. L., Janssens, S., Crijns, H. J., & Moens, A. L. (2012). Doxorubicin-induced Cardiomyopathy: From Molecular Mechanisms to Therapeutic Strategies. *Journal of Molecular and Cellular Cardiology*, 52(6), 1213–1225.

Olson, R. D., Boerth, R. C., Gerber, J. G., & Nies, A. S. (1981). Mechanism of Adriamycin Cardiotoxicity: Evidence for Oxidative Stress. *Life Sciences*, 29(14), 1393–1401.

Park, J. H., Choi, S. H., Kim, H., Ji, S. T., & Jang, W. B. (2016). Doxorubicin Regulates Autophagy Signals via Accumulation of Cytosolic Ca 2 + in Human Cardiac Progenitor Cells. *International Journal of Molecular Sciences,* 17(1680), 1–13.

Patterson, C., Ike, C., Willis (IV), P.W., Stouffer, G.A., & Willis, M.S. (2007). The Ubiquitin-Proteasome System and Cardiac Dysfunction. *Circulation,* 115, 1456–1463

Pizarro, M., Troncoso, R., Martinez, G., Mario, C., Pablo F. C., & Lavandero, S. (2016). Basal Autophagy Protects Cardiomyocytes from Doxorubicin-induced Toxicity. *Toxicology*, 370 (October), 41–48.

Powell, S.R., (2006). The Ubiquitin- Proteasome System in Cardiac Physiology and Pathology. *The American Journal of Physiology: Heart and Circulatory Physiology*, 291, 1–19.

Raffaghello, L., Lee, C., Safdie, F. M., Wei, M., Madia, F., Bianchi, G., & Longo, V. D. (2008). Starvation-dependent Differential Stress Resistance Protects Normal but Not Cancer Cells Against High-dose Chemotherapy. *The National Academy of Sciences of the USA*, 105(24), 8215–8220

Rahman, A., Carmichael, D., Harris, M. & Roh, J.K. (1986). Comparative Pharmacokinetics of Free Doxorubicin and Doxorubicin Entrapped in Cardiolipin Liposomes. *Cancer Research*, 46, 2295–2299.

Roach, P. J. (2011). Commentary, AMPK- ULK1- Autophagy. *Molecular and Cell Biology*, 31(15), 3082-3084.

Seidman, A., Hudis, C., Pierri, M. K., Shak, S., Paton, V., Ashby, M., & Keefe, D. L. (2002). Cardiac Dysfunction in the Trastuzumab Clinical Trials Experience. *Journal of Clinical Oncology*, 20, 1215–1221.

Shan K., Lincoff M., &Young J. B. (1996). Anthracycline-induced cardiotoxicity. *Annals of Internal Medicine*, 125, 47–58.

Šimùnek, T., Štěrba, M., Popelová, O., Adamcová, M., Hrdina, R., & Geršl, V., (2009). Anthracycline-induced Cardiotoxicity: Overview of Studies Examining the Roles of Oxidative Stress and Free Cellular Iron. *Pharmacol Rep* 61, 154–171.

Sishi, B. J. N., Loos, B., Rooyen, J. Van., & Engelbrecht, A. M. (2013). Autophagy Upregulation Promotes Survival and Attenuates Doxorubicin-induced Cardiotoxicity. *Biochemical Pharmacology*, 85(1), 124–134.

Smuder, A. J., Kavazis, A. N., Min, K., Powers, S. K., Aj, S., & An, K. (2013). Doxorubicin-induced Markers of Myocardial Autophagic Signalling in Sedentary and Exercise Trained Animals. *Journal of Applied Physiology*, 115, 176–185.

Steinhubl, S. R. (2008). Why Have Antioxidants Failed in Clinical Trials? *The American Journal of Cardiology*, 101(10A), 14–19.

Sterba, M., Popelova, O., Vavrova, A., Jirkovsky, E., Kovarikova, P., Gersi, V., & Šimůnek, T. (2013). Oxidative Stress, Redox Signalling, and Metal Chelation in Anthracycline Cardiotoxicity and Pharmacological Cardioprotection. *Antioxidants & Redox Signalling*, 18(8), 899–929.

Sun, A., Cheng, Y., Zhang, Y., Zhang, Q., Wang, S., Tian, S., & Zou, Y. (2014). Aldehyde Dehydrogenase 2 Ameliorates Doxorubicin-induced Myocardial Dysfunction Through Detoxification of 4-HNE and Suppression of Autophagy. *Journal of Molecular and Cellular Cardiology*, 71(2014), 92–104.

Swain, S. M., Whaley, F. S., & Ewer, M. S. (2003). Congestive Heart Failure in Patients Treated with Doxorubicin: A Retrospective Analysis of Three Trials. *Cancer*, 97(11), 2869–2879.

Tacar, O., Sriamornsak, P., & Dass, C. R. (2012). Doxorubicin: An Update on Anticancer Molecular Action, Toxicity and Novel Drug Delivery Systems. *Journal of Pharmacy and Pharmacology*, (65), 157–170.

Takemura, G., & Fujiwara, H. (2007). Doxorubicin-Induced Cardiomyopathy. From the Cardiotoxic Mechanisms to Management. *Progress in Cardiovascular Diseases*, 49(5), 330–352.

Takeshige, K., Baba, M., Tsuboi, S., Noda T., & Ohsumi, Y. (1992). Autophagy in Yeast Demonstrated with Proteinase-deficient Mutants and Conditions for its Induction. The Journal of Cell Biology, 119(2), 301-311.

Tewey, K. M., Chenb, G. L., Nelsonf, E. M., & Lius, L. F. (1984). Intercalative Antitumor Drugs Interfere with the Breakage-Reunion Reaction of Mammalian DNA Topoisomerase II. *The Journal of Biological Chemistry,* 259(14), 9182–9187.

Vejpongsa, P., & Yeh, E. T. H. (2014). Prevention of Anthracycline-Induced Cardiotoxicity. *Journal of the American College of Cardiology*, 64(9), 938–945.

Vezina, C., Kudelski, A., & Sehgal, S. N. (1975). Rapamycin (AY-22,989), A New Antifungal Antibiotic. Taxonomy of the Producing Streptomycete and Isolation of the Active Principle. *The Journal of Antibiotics*, 28(10), 721–726.

Von Hoff, D. D., Layard, M. W, Basa., P, Davis, H. L., Von Hoff, A. L., Rozencweig, M., & Muggia, F. M. (1979). Risk Factors for Doxorubicin-induced Congestive Heart Failure. *Annals of Internal Medicine.*

Wang, X., Chen, H., Wu, D., Chen, J., Wang, X., & Jiang, W. (2014). Ghrelin Inhibits Doxorubicin Cardiotoxicity by Inhibiting Excessive Autophagy Through AMPK and p38-MAPK. *Biochemical Pharmacology,* 88, 334–350

Weng, L., Zhang, W., Ye, Y., Yin, P., Yuan, J., Wang, X., & Jiang, S. (2014). Aliskiren Ameliorates Pressure Overload-induced Heart Hypertrophy and Fibrosis in Mice. *Nature Publishing Group,* 35(8), 1005–1014.

Willis, M.S., & Patterson, C., (2006). Into the heart: The Emerging Role of The Ubiquitin-Proteasome System. *Journal of Molecular and Cellular Cardiology*. 41, 567–579.

World Health Organization. (2017). WHO Model List of Essential Medicines, 20(March).

Xu, X., Chen, K., Kobayashi, S., Timm, D., & Liang, Q. (2012). Resveratrol Attenuates Doxorubicin-Induced Cardiomyocyte Death via Inhibition of p70 S6 Kinase 1-Mediated Autophagy. *The Journal of Pharmacology and Experimental Therapeutics*, 341(1), 183–195.

Yan, L., Vatner, D. E., Kim, S., Ge, H., Masurekar, M., Massover, W. H., & Vatner, S. F. (2005). Autophagy in Chronically Ischemic Myocardium. *The Nation Academy of Sciences of the USA*, 102(39), 13807–13812.

Yang, S. S., Liu, Y.B., Yu, J. B., Fan, Y., Tang, S. Y., Duan, W. T, Wang, Z., Gan, R. T., & Yu, B. (2010). Rapamycin Protects Heart from Ischemia/ Reperfusion Injury Independent of Autophagy by Activating PI3 kinase-Akt Pathway and Mitochondria KATP channel. *Pharmazie*, 65(10), 760–765.

Yang, Y., Hu, L., Zheng, H., Mao, C., Hu, W., Xiong, K., & Wang, F. (2013). Application and Interpretation of Current Autophagy Inhibitors and Activators. *Nature Publishing Group*, 34(5), 625–635.

Zhang, W., Deng, J., Sunkara, M., Morris, A. J., Wang, C., Clair, D. S., & Vore, M. (2015). Loss of Multidrug Resistance - Associated Protein 1 Potentiates Chronic Doxorubicin-Induced Cardiac Dysfunction in Mice. *The Journal of Pharmacology and Experimental Therapeutics*, 355(November), 280–287.

Zhang, Y. W., Shi, J., Li, Y. J., & Wei, L. (2009). Cardiomyocyte Death in Doxorubicin-induced Cardiotoxicity. *Archivum Immunologiae et Therapiae Experimentalis*, (57), 435–445.

Zhou, S., Palmeira, C. M., & Wallace, K. B. (2001). Doxorubicin-induced Persistent Oxidative Stress to Cardiac Myocytes. *Toxicology Letters*, 121(3), 151–157.

Zitka, O., Skalickova, S., Gumulec, J., Masarik, M., Adam, V., Hubalek, J., & Kizek, R. (2012). Redox Status Expressed as GSH: GSSG Ratio as a Marker for Oxidative Stress in Paediatric Tumour Patients. *Oncology Letters*, 4, 1247–1253.

Zweier, J. L. (1984). Reduction of 02 by Iron Adriamycin. *The Journal of Biological Chemistry*, 259(10), 6056–6059.

Zweier, J. L., Gianni, L., Muindi, J., & Myers, C. E. (1986). Differences in O2 Reduction by the Iron Complexes of Adriamycin and Daunomycin: The importance of the Sidechain Hydroxyl Group. *Biochimica et Biophysica Acta*, 884, 326–336.

Appendix A

Table A1: Food consumed in grams

	Control	Rapamycin	Starvation	DOX	DOX+ rapa	Dox+ starve
Week 1	x	x	x	x	x	x
Week 2	139.43	169.14	144.52	155.34	144.45	143.60
Week 3	164.25	152.93	124.40	175.44	159.80	154.18
Week 4	185.93	167.18	124.50	173.72	153.33	179.99
Week 5	181.73	164.40	123.00	180.31	157.27	170.51
Week 6	197.25	167.55	135.90	181.85	153.59	201.54
Week 7	198.68	159.00	138.00	177.42	152.57	172.55
Week 8	236.03	200.63	148.00	191.36	165.00	205.45
Week 9	225.98	204.45	152.10	182.44	156.60	177.68
Week 10	213.45	195.53	136.50	174.36	150.47	169.78

Table A2: Animal mass over time in grams

		Control	Rapamycin	Starvation	DOX	DOX+ rapa	Dox+ starve
Week 1	Mean	21.1000	19.3000	19.2667	19.5333	20.5500	20.1500
	SEM	0.7257	1.4615	1.5720	0.6380	0.9588	0.8530
Week 2	Mean	23.2167	21.2833	20.0667	21.8167	23.2167	22.5167
	SEM	0.7355	1.7772	2.0816	0.7030	0.8460	0.9581
Week 3	Mean	25.0000	22.3667	20.7000	22.9167	22.9167	23.1833
	SEM	0.7685	2.0013	2.2802	0.7562	0.7562	1.0717
Week 4	Mean	26.2333	22.9833	21.2167	23.8167	23.6167	23.9167
	SEM	0.7584	2.0816	2.3034	0.8590	0.8717	1.1620
Week 5	Mean	27.3833	24.1167	22.3833	24.4333	24.2000	24.5500
	SEM	0.7609	2.1388	2.1425	0.8395	0.9441	1.3061
Week 6	Mean	28.3000	24.8167	22.9167	24.5000	24.3500	24.8333
	SEM	0.7971	2.0905	2.2470	0.8983	0.9081	1.2820
Week 7	Mean	28.7167	25.8000	23.6167	24.5500	24.7167	24.4500
	SEM	0.6353	1.8826	2.2261	0.7782	0.9245	1.1316
Week 8	Mean	29.4833	26.9333	24.0667	24.9167	25.2333	25.4333
	SEM	0.8203	1.7046	2.2917	0.7818	1.0415	1.2843
Week 9	Mean	30.1667	28.0000	24.7167	24.9667	25.5833	25.1833
	SEM	0.8119	1.8857	2.1499	0.7533	1.1256	1.1698
Week 10	Mean	30.4167	28.0000	24.8167	25.3833	25.5667	25.5000
	SEM	0.6630	1.8834	2.2279	0.8874	1.1659	1.1922

Table A3: Organ mass in grams

		Control	Rapamycin	Starvation	DOX	DOX+ rapa	Dox+ starve
Heart	Mean	0.1845	0.1683	0.1275	0.1693	0.1452	0.1527
	SEM	0.0253	0.0199	0.0179	0.0144	0.0123	0.0146
Liver	Mean	1.5883	1.4118	1.1608	1.3070	1.3379	1.3290
	SEM	0.0837	0.1208	0.1180	0.0455	0.0876	0.0543
Pancreas	Mean	0.2358	0.2877	0.3248	0.2993	0.3097	0.2997
	SEM	0.0303	0.0388	0.0568	0.0129	0.0395	0.0191
Kidney	Mean	0.1963	0.2340	0.1673	0.1543	0.1675	0.1760
(right)	SEM	0.0140	0.0560	0.0141	0.0067	0.0086	0.0054
Kidney	Mean	0.2047	0.1908	0.1663	0.1743	0.1785	0.1755
(left)	SEM	0.0120	0.0173	0.0121	0.0062	0.0069	0.0077

Table A4: Various muscle mass in grams

		Control	Rapamycin	Starvation	DOX	DOX+ rapa	Dox+ starve
gastrocnemius	Mean	0.1385	0.1300	0.1213	0.1258	0.1440	0.1277
(right)	SEM	0.0119	0.0146	0.0113	0.0078	0.0084	0.0121
gastrocnemius	Mean	0.1298	0.1292	0.1240	0.1272	0.1270	0.1283
(left)	SEM	0.0154	0.0092	0.0147	0.0086	0.0061	0.0107
soleus	Mean	0.0117	0.0086	0.0075	0.0098	0.0085	0.0065
(right)	SEM	0.0009	0.0022	0.0010	0.0016	0.0015	0.0010
soleus	Mean	0.0114	0.0105	0.0097	0.0075	0.0083	0.0088
(left)	SEM	0.0028	0.0017	0.0016	0.0019	0.0018	0.0011
plantaris	Mean	0.0116	0.0063	0.0098	0.0112	0.0120	0.0090
(right)	SEM	0.0037	0.0014	0.0035	0.0019	0.0021	0.0023
plantaris	Mean	0.0143	0.0087	0.0077	0.0087	0.0115	0.0120
(left)	SEM	0.0032	0.0027	0.0027	0.0020	0.0022	0.0023

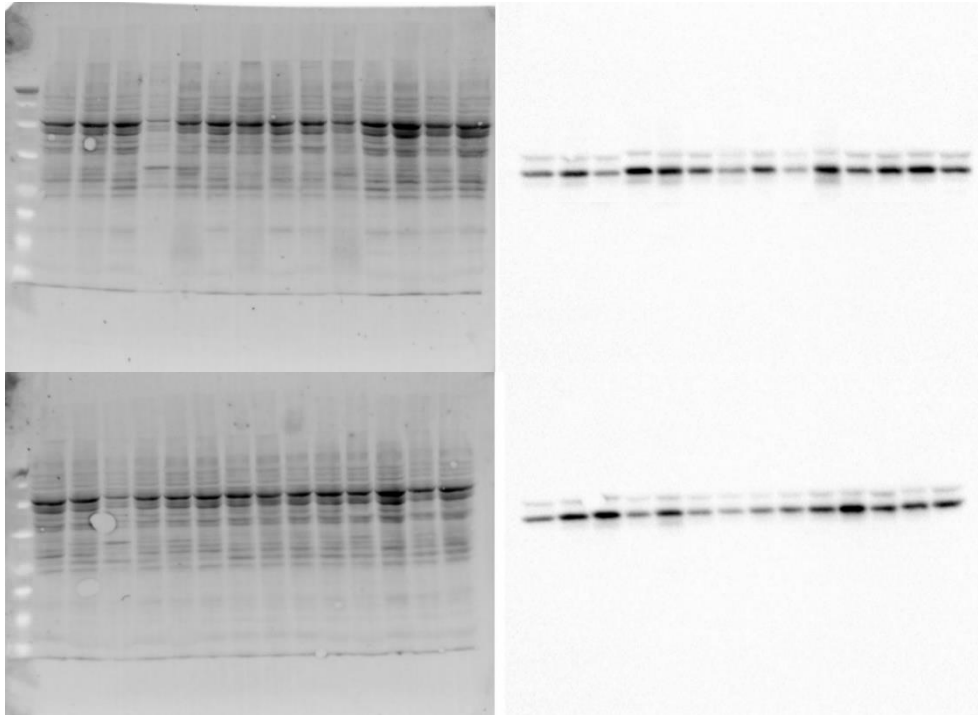Figure A1: Caspase 3 total protein and bands detected. Left: Total protein. Right: Bands visualised. Rows (from left to right); C, R, S, D, D+ R, D+S, C, R, S, D, D+ R, D+S, D, D+ R.
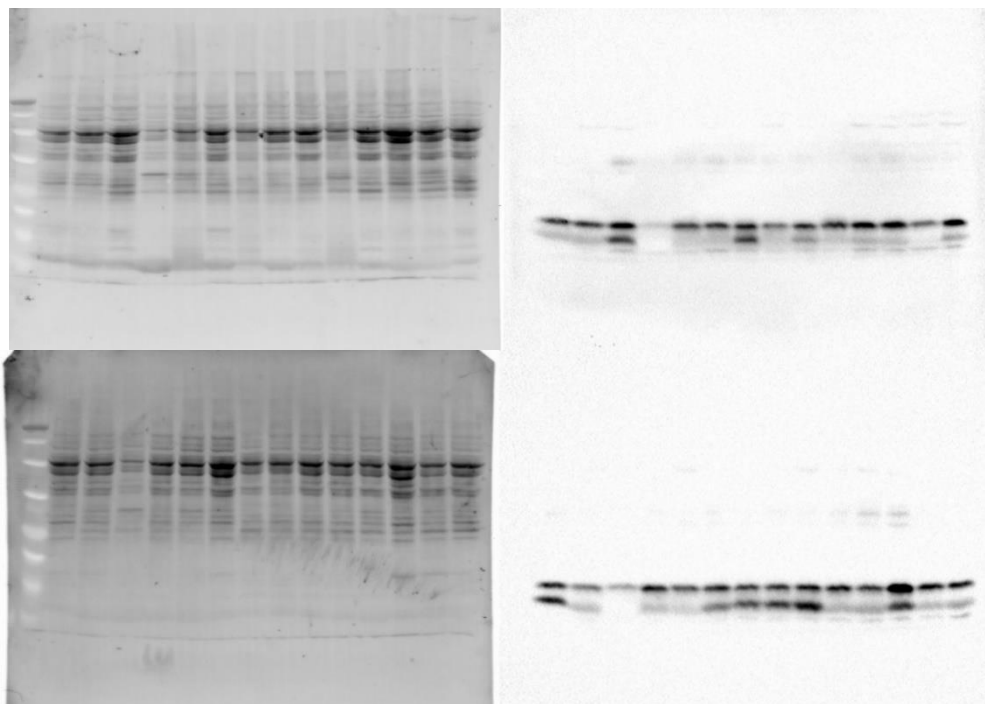
Figure A2: LC3 total protein and bands detected. Left: Total protein. Right: Bands visualised, top band 16kDa LC3I, bottom band 14kDa LC3II. Rows (from left to right); C, R, S, D, D+ R, D+S, C, R, S, D, D+ R, D+S, D, D+ R.

Appendix B

Full protocols used during this study:

Animal work

The in vivo study was conducted on a total of 39 male black 6 (C57BL/6) mice. The study however was staggered. Mice were received after weaning at 3 weeks. Initially 20 mice were received from the Research Animal Facility, Faculty of Health Sciences, University of Cape Town and Animal Unit, Stellenbosch University, Tygerberg Campus. Overlapping the first study 20 more mice were received. Mice were left to acclimatise to the animal house at the University of Stellenbosch in the cages in which they arrived. The mice were kept on a 12-hour day- night cycle, fed a standard rodent chow (LabChef, Rodent Breeder) and given free access to food and water.

Mice were then randomly split into groups; control, rapamycin, starvation, doxorubicin, dox-rapa combination and dox- starve combination groups respectively. The rats were left for 3 weeks to acclimatize within their respective group. During this acclimation period 1 mouse died, prior to receiving any treatment. The total amount of animals per group were as followed:

Control   6

Rapamycin   6

Starvation   6

Doxorubicin   7

Dox- Rapa   7

Dox- Starve   7

24 hours before the treatment the animals were weighed, food was taken from the starvation and the dox and starve groups at this time point. The average weight of the group was used to calculate the dosage.

The control group each received a 200µL injection of saline solution, administered via intraperitoneal injection. The rapamycin group received 2mg/kg of rapamycin solution (LKT laboratories, R0161), made up to a volume of 200µL, administered via intraperitoneal injection. The doxorubicin group received 2mg/kg of doxorubicin hydrochloride (LKT laboratories D5794) solution, made up to a volume of 200µL, administered via intraperitoneal injection. The dox- rapa combination group received 2mg/kg of rapamycin solution, made up to a volume of 200µL, administered via intraperitoneal injection then 30 minutes later, 2mg/kg of doxorubicin solution, made up to a volume of 200µL, also administered via intraperitoneal injection. The dox- starve combination group received 2mg/kg of doxorubicin solution, made up to a volume of 200µL, 24 hours after food was withheld, administered via intraperitoneal injection. The food was restored to the starvation group and the dox- starve group after 24 hours. These treatment protocols continued for a total of 8 weeks, no animals were lost as a result of treatment. All injections were done using a new 29G x ½" 1mL insulin syringe. A week after the final treatment the animals were euthanized via cervical dislocation. Following euthanasia, the chest was opened, and the heart harvested. The removal of the heart was necessary for the study as well as serving as confirmation of death. Hearts were sectioned coronally, roughly in half. One section was flash frozen in liquid nitrogen, then stored at -80°C. The other section was preserved in a 4% buffered formaldehyde (approximately 10% formalin) solution.

Staining

Staining was performed on the tissue preserved in formaldehyde.

Tissue processing

Tissue processing was done automatically using a Tissue-Tek II tissue processor, using the following protocol:

Dehydration

1.	70% alcohol	1.5 hrs
2.	70% alcohol	1.5 hrs
3.	90% alcohol	1.5 hrs
4.	95% alcohol	1.5 hrs
5.	95% alcohol	1.5 hrs
6.	100% alcohol	1.5 hrs
7.	100% alcohol	1.5 hrs
8.	100% alcohol	2 hrs

Clearing

9.	Xylene	1.5 hrs
10.	Xylene	2 hrs

Impregnation

11.	Paraffin wax	2 hrs
12.	Paraffin wax	2 hrs

Total time	20 hrs

Paraffin wax was purchased from Sigma- Aldrich (P3558 Paraplast).

Embedding

After processing the tissue was embedded in paraffin wax. Embedding was done using a Leica EG1150 H paraffin embedding station.

Sectioning

The tissue was sectioned using a Lecia RM 2125 RT microtome, at a 2º angle and 5µM thickness. 3 serial sections were taken for each sample. These sections were transferred to a

water bath ±40ºC then picked up onto a glass slide then placed in a 65ºC oven for roughly 5 minutes.

Staining

Staining was performed at the University of Stellenbosch Medical Campus, Tygerberg. Haematoxylin and eosin staining was done automatically using a Leica ST5010 Autostainer XL, using the following protocol:

1.	Xylene	5 minutes
2.	Xylene	5 minutes
3.	99% alcohol	2 minutes
4.	99% alcohol	2 minutes
5.	96% alcohol	2 minutes
6.	70% alcohol	2 minutes
7.	Tap water	2 minutes
8.	Haematoxylin	8 minutes
9.	Running water	5 minutes
10.	Eosin	4 minutes
11.	Running water	1 minutes
12.	70% alcohol	30 seconds
13.	96% alcohol	30 seconds
14.	96% alcohol	30 seconds
15.	99% alcohol	30 seconds
16.	Xylene	1 minutes

Total time   41 minutes

After staining allow slides to dry then mount cover slip with DPX.

Picrosirius red staining was done by hand, using the following protocol:

1.	Xylene	5 minutes
2.	Xylene	5 minutes
3.	99% alcohol	2 minutes
4.	99% alcohol	2 minutes
5.	96% alcohol	2 minutes
6.	70% alcohol	2 minutes

7.	Tap water	2 minutes
8.	Weigert's haematoxylin	12 minutes
9.	Running tap water	10 minutes
10.	Picrosirius red	60 minutes
11.	Acidified water	2 minutes
12.	Acidified water	2 minutes
13.	100% alcohol	5 dips
14.	100% alcohol	5 dips
15.	100% alcohol	5 dips
16.	Xylene	1 minutes
17.	Xylene	2 minutes

Total time $\pm$ 110 minutes

After staining allow slides to dry then mount cover slip with DPX.

Sections were analysed using a Nikon Eclipse E4000 microscope and NIS Elements imaging software (version 4.10).

Haematoxylin and eosin stains were photographed at 40x using a Nikon DS-Fi2 camera. These micrographs were stitched together using the NIS Elements to create an image of the entire organ. This whole image was used to assess any major structural abnormalities.

Picrosirius red sections were photographed at 400x, random areas were photographed. Each group had 15 random images taken. The images were analysed using ImageJ software (version 1.49) using the following protocol:

1. File- Open   [ctrl + O]
2. Image- Adjust.

    Brightness/ Contrast   [ctrl + Shift + C]

    Set- Set Display Range.

    Adjust minimum and maximum display values to clarify image

3. Image- Adjust.

    Threshold   [ctrl + Shift + T]

    Adjust hue, saturation and brightness to select entire tissue (red and yellow)

4. Analyse- Measure   [ctrl + M]

    This measurement is the Total Tissue Area

5. Image- Adjust.

    Threshold   [ctrl + Shift + T]

    Adjust hue, saturation and brightness to select red tissue only

6. Analyse- Measure   [ctrl + M]

    This measurement is the Red Tissue Area

This method measures the area of the red stain rather than the colour intensity to calculate fibrosis. Fibrosis was calculated as such:

$$\frac{Red\ Tissue\ Area}{Total\ Tissue\ Area} \times 100 = Fibrous\ \%$$

Oxidative stress

Fluorometry was performed on some of the frozen tissue. These assays were performed at the Oxidative Stress Research Centre, Cape Peninsula University of Technology, Bellville. Lysates were prepared for the oxidative stress fluorometric assay according to the following protocol:

1. Defrost frozen tissue slowly by placing on ice
2. Tissue was weighed and placed into a labelled Eppendorf tube
   a. 15mg for GSH and CDs
   b. 10mg for GSSG
3. To GSH add phosphate buffer (1000µl per 100mg tissue)
   For 15mg add 150µl
4. To GSSG add 1% M2VP phosphate buffer solution (1000µl per 100mg)
   For 10mg add 100µl
5. Homogenise tissue
6. Wait for froth to settle (±30 minutes)
7. Centrifuge at 12 000rpm for 10 minutes
8. Transfer supernatant into a new Eppendorf tube (discard pellet)

These lysates were used for the GSH, GSSG and CDs assays. The lysates may be stored at -80ºC and used at a later stage. After pilot testing a dilution factor of 20 was calculated appropriate. The GSH/ GSSG assay was performed using the following protocol:

1. Load the appropriate amount of GSH standard solution (3µM GSH) into the first wells of a 96-well plate (in triplicate)
2. Load the appropriate amount of phosphate buffer solution into the corresponding wells of the plate

	Blank	1	2	3	4	5
Standard solution (µL)	0	167	333	500	667	833
Phosphate buffer (µL)	1000	833	667	500	333	167
Concentration	0	0,5	1,0	1,5	2,0	2,5

3. Load 50µL of sample to the wells of a 96-well plate (in triplicate)
4. Load 50µL DTNB to each well using multichannel pipette
5. Load 50µL glutathione reductase to each well using multichannel pipette

65

6. Load 50µL NADPH to each well as quickly as possible to each well using multichannel pipette

7. Measure absorbance at 412nm every 30 seconds for 3 minutes using a Fluoroskan Ascent Microplate Fluorometer (Thermo Fisher Scientific)

Absorbance readings were analysed, Microsoft Excel was used to average triplicates and GraphPad Prism (version 6.01) was used to generate a standard curve. The time of measurement was plotted on the X axis and the absorbance of each standard was plotted on the Y axis of a line graph. Linear regression was used to calculate the slope of each standard. This was used to generate the standard curve; the concentration of each standard was plotted on the X axis and the slope of each standard was plotted on the Y axis of a line graph. Linear regression was used to calculate the slope of the standard curve.

To calculate the concentration of each sample a slope must be generated for each sample. The time of measurement was plotted on the X axis and the absorbance of each sample was plotted on the Y axis of a line graph. Linear regression was used to calculate the slope of each sample. The slope was used as the Y, the M and C were taken from the standard curve allowing as to calculate the X by rearranging the formula for a straight line.

$$Y = MX + C$$

$$\frac{Y - C}{M} = X$$

This however is the concentration in µM. To convert the unit to µM/g, the concentration (µM) must be multiplied by the dilution factor and the volume of the sample (L) and divided by the weight of tissue (g).

$$\mu M/g = \mu M \times DF \times L/g$$

The above calculation is for GSH. To calculate GSSH simply divide the answer by 2.

$$\mu M/g = \mu M \times DF \times L/g \div 2$$

To perform the conjugated dienes (CDs) assay, lysates from the GSH group were modified according to the following protocol:

1. Add 300µL chloroform and 600µL methanol together to form a solution
2. Add 250µL of this solution to 50µL of lysate sample in an Eppendorf tube
3. Invert Eppendorf tube to mix

4. Centrifuge at 14 000rpm for 1minutes

5. Pipette 200µL of the bottom layer of liquid into a new Eppendorf tube

6. Leave tubes open, refrigerate overnight (±12 hours) at 4ºC

7. Add 1mL cyclohexane to each Eppendorf tube, vortex for 20s

8. Load 300µL blank into the wells of a UV clear 96-well plate (in triplicate)

8. Load 300µL of each sample into the wells (in triplicate)

9. Measure absorbance at 380nm using a Fluoroskan Ascent Microplate Fluorometer (Thermo Fisher Scientific)

Absorbance readings were analysed, Microsoft Excel was used to average triplicates. For the CD's there is no standard curve. The concentration was calculated by dividing absorbance by the excitation coefficient.

$$Concentration = \frac{(absorbance\ of\ sample\ - absorbance\ of\ blank)}{excitation\ coefficient\ (29500)}$$

Western blot

Western blots were performed on some of the frozen tissue.

Lysates were prepared for the western blot assays according to the following protocol:

1. Defrost frozen tissue slowly by placing on ice
2. Tissue was weighed and placed into a labelled Eppendorf tube
    a. 10-15mg
3. Add 100µL of working RIPA buffer to each Eppendorf tube
    a. 100µL per 10mg
    b. 100µL per 15mg preferred
4. Homogenize tissue on ice
    a. Rinse homogenizer with distilled H_2O, then working RIPA buffer
5. Wait roughly an hour for froth to settle
6. Centrifuge at 4ºC at 14 000rpm for 15minutes
7. Remove supernatant into new Eppendorf tube
8. Centrifuge at 4ºC at 14 000rpm for 15minutes
9. Remove supernatant into new Eppendorf tube
10. Pipette 2ul of RIPA buffer on a Direct Detect Spectrometer assay free card as the blank
11. Pipette 2ul of each sample onto the cards
    a. Select protein
    b. Select RIPA calibration curveq3
12. Measure protein concentration on Direct Detect Spectrometer
    a. Using that value, the sample protein concentration (X), the following can be calculated:
    b. The amount of sample needed to prepare 30µg of protein per lysate:
$$Amount\ in\ \mu L = (30 \times 1000) \div (X) \times 1000$$
    c. The amount of working RIPA buffer to be added:
$$Amount\ in\ \mu L = 10 - [(30 \times 1000) \div (X) \times 1000]$$
13. Prepare lysate to a total volume of 20µL by adding:
    a. Amount of sample to prepare 30µg of protein, calculated by the equation above
    b. Amount of working RIPA, calculated by equation the above
    c. 15µL of Laemmli's buffer
14. Once all lysates are prepared, boil each for 5minutes at 95°C

15. Store lysates at -80ºC

Western blots were run according to the following protocol:

1. Take lysates out freezer
    a. Thaw on ice
2. Boil lysates for 5minutes at 95˚C
3. Centrifuge at 9300 RPM
4. Place back on ice
5. Place the assembly in a gel tank
    a. Fill the buffer dam with cold 1x running buffer until it spills into the tank
    b. Top up the tank until the buffer is level with the buffer at the top of the dam (the dam is the empty area between the two gel plates, if running 2 gels or between the one plate and the buffer dam plate, when only 1 gel is being run)
6. Wash the wells with running buffer, using an insulin syringe.
7. Load wells [15 well can take max 26ul]
    a. Load 3µl of protein marker to the first lane on the far left of each gel
    b. Load 13.34µl lysate per well to ensure 20µg protein per lane
8. Run gels
9. Place the green lid with appropriate leads
    a. Black to black: red to red
    b. Connect to the power pack
    c. 100V, 400mA for ±3 hours
10. Switch off power and disconnect electrodes. Remove gel plates from the tank and proceed to electro transfer step immediately

Transferring to membrane

1. Use trans-blot turbo RTA transfer kit
    a. Soak blotting paper in transfer buffer
    b. Soak membrane in methanol for a few seconds then
    c. Soak membrane in transfer buffer for ±5 minutes
2. Activate on chemidoc
3. Place in trans-blot turbo transfer system cassestte
4. Transfer on mmw for 7 minutes
5. Image on chemidoc
6. Rinse membrane on shaker
    a. 3x 5 minutes stripping buffer
7. Block for 2 hours in 5% milk on shaker
8. Place in 50mL tube containing 5mL of primary antibody
    a. Leave on rotator in 4ºC walk in fridge for 72 hours
9. Remove membrane from primary antibody
10. Rinse membrane in 1x TBS-T
11. Place in secondary antibody
    a. Leave on rotator at room temperature for 1 hour
12. Rinse membrane in TBS-T
13. In foil covered tube, prepare ECL in 1:1 ratio (0.5ul: 0.5ul = per membrane)
14. Pour ECL over membrane, focusing on MW area of protein
    a. Incubate for 5 minutes
15. Image
    a. Open "image lab"
    b. Select 'blot' then 'chemi'
    c. Do not overexpose protein of interest
    d. Image ladder to confirm molecular weight of protein
    e. Save images

Appendix C

List of reagents used during this study:

Animal work

1. Doxorubicin

2. Rapamycin

1. Doxorubicin was prepared as such:
   - 10mg dry powder was dissolved in 5mL of saline solution and vortexed until the powder was fully dissolved.
   - This solution was further diluted by adding an additional 20mL of saline solution. Bringing the total volume to 25mL and the concentration to 400µg/mL.

$$400\mu g/mL = 2000\mu g/5mL$$

$$2mg/5mL = 2000\mu g/5mL$$

As each animal receives 2mg/kg

$$2mg/5mL \ and \ 2mg/kg \ \therefore \ 5mL/kg$$

$$5mL/kg \ = \ 5uL/g$$

Therefore, the equation to calculate dose would be as follows:

$$average \ weight \ in \ gram \ \times 5uL \ = dose \ per \ animal$$

$$dose \ per \ animal \ \times (n+1) = total \ dose \ per \ group$$

$$(n+1) \times 200uL - total \ dose \ per \ group = amount \ of \ diluent$$

(n + 1) is used to prepare an extra dose in case of emergency

200µL is used as the total injection volume

If, for example, the average weight of the group containing 4 mice is 21.6 grams then:

$$21.6g \times 5\mu L = 108uL$$

$$108\mu l \ \times 6 = 648uL$$

$$1200uL - 648uL = 552uL$$

648µL of doxorubicin solution was mixed with 552µL of saline solution. Each mouse then received 200µL of this solution.

2. Rapamycin was prepared as such:

    - 10mg dry powder was dissolved 2mL of 70% alcohol and vortexed until the powder was fully dissolved, 23mL of saline solution was also added. Bringing the total volume to 25mL and the concentration to 400µg/mL. The rapamycin solutions were then prepared in the same manner as the doxorubicin solutions.

Oxidative stress

The solutions required for the assays:

1. Phosphate buffer (75mM)
2. NADPH (1mM) in phosphate buffer
3. M2VP (30mM) in 0.1M HCl
4. DTNB (0.3mM) in phosphate buffer
5. Glutathione reductase (16 µL in 984 µL phosphate buffer)

1. Phosphate buffer was prepared as such:

    - 1st solution
        - 1,035g Sodium phosphate monobasic monohydrate ($NaH_2PO_4.H_2O$) in 100ml of distilled H_2O and mix until dissolved.
    - 2nd solution
        - 1,335g di-Sodium hydrogen phosphate anhydrous (Na_2HPO_4) in 100ml of distilled H_2O and mix until dissolved.
    - Mix 18ml of the 1st solution with 82ml of the 2nd solution.
    - Adjust pH to pH 7.5
    - Store at 4ºC

Western blot

The solutions required for the preparation of the lysates for the western blot assay:

1. Working RIPA buffer
2. Laemmli's buffer

1. To prepare working RIPA:

- Add 1mL RIPA buffer to an Eppendorf tube

- Add 42ul Protease Cocktail

- Add 10ul PMSF

- Add 5ul NaF

- Add 5ul Sodium Orthovandate (Na$_3$VO$_4$)

- Vortex to mix and keep on ice during use

To prepare RIPA buffer:

- Add 790 mg Tris base to 75 ml dH$_2$O.

- Add 900 mg NaCl and stir solution until all solids are dissolved.

  o Using HCl, adjust pH to 7.4

- Add 10 ml of 10 % NP-40 to solution

- Add 2.5 ml of 10 % Na-deoxycholate and stir until solution is clear

- Add 1 ml of 100 mM EDTA to the solution.

- Adjust the volume of solution to 100 ml using a graduated cylinder

To prepare the RIPA reagents:

10 % NP-40

- Dissolve 1g NP-40 powder into 10 ml dH$_2$O in a foil wrapped flask
- Place a stirrer in beaker and place beaker on heated magnetic stirrer until powder is completely dissolved

10% Na-deoxycholate

- Dissolve 0.5g Na-deoxycholate powder into 5 ml dH$_2$O

100 mM EDTA

- 404.47g/1000ml = 1M = 1000mM
    - 40.447g/1000ml =100mM
- Therefore 20.22g/500ml =100mM
- Make up to 400ml, adjust pH to pH7.4
- Adjust to 500ml

2. To prepare Laemmli's buffer:

- Add 850ul Laemmli's stock solution to a foil wrapped flask
- Add 150ul 2-Mercaptoethanol in fume hood

To prepare the Laemmli's stock:

- Add 38ml distilled H_2O to a foil wrapped flask
- Add 10ml 0.5M Tris
    - use HCl to adjust pH to pH6.8
- Add 8ml glycerol
- Add 16ml 10% SDS
- Add 4ml 0.05% (w/v) Bromophenol blue

To prepare the Laemmli's stock reagents:

0.5M Tris

- Add 6.057g of Tris to 70ml distilled H_2O
    - adjust pH to pH6.8
- Make up to 100ml

10% SDS

- Add 2g SDS to 20ml distilled H_2O

0.05% (w/v) Bromophenol blue

- Add 2,5mg bromophenol to 5ml distilled H_2O

The solutions required for the preparation of the lysates for the western blot assay:

1. Resolving gel
2. Stacking gel
3. Running buffer
4. Transfer buffer
5. TBST

1. 12% resolving gel (2 gels)
   - To a small beaker
     - Add 5.7mL distilled H_2O
     - Add 4.5mL 40% acrylamide solution
     - Add 3.75mL 1.5M Tris-HCl (pH8.8)
     - Add 150µL 10% w/v SDS
     - Add 75µL TCE
   - Swirl gently to mix
     - Add 150µL 10% w/v APS
   - Swirl gently to mix
     - Add 6µL of TEMED
   - Swirl gently to mix
   - Using a plastic Pasteur pipette quickly pour between to plates, pour from one corner to avoid bubble, leaving space for stacking gel
   - Top with a layer of EtOH
   - Allow gel to set
     - 30-60 minutes
   - Once gel has set, pour off EtOH, dab dry with blotting paper
2. 4% stacking gel (2 gels)
   - To a small beaker
     - Add 4.48mL distilled H_2O
     - Add 1mL 40% acrylamide solution
     - Add 2mL 0.5M Tris-HCl (pH6.8)
     - Add 80µL 10% w/v SDS
   - Swirl gently to mix

- o Add 80µL 10% w/v APS
- Swirl gently to mix
  - o Add 8µL of TEMED
- Swirl gently to mix
- Using a plastic Pasteur pipette quickly pour between to plates, pour from one corner to avoid bubble, leaving space for comb.
- Insert comb gently, pushing down and avoiding bubble formation
- Allow gel to set

3. Running buffer
   - 100ml 10x running buffer
   - 900ml dH20

10x running buffer

- 60.6g Tris
- 288g Glycine
- Dissolve Tris and Glycine in 1.5L dH20 (±1 hr)
  - o Adjust pH to pH8.6
- Add 20g SDS
- Add dH2O until 2L

4. Transfer buffer
   - 200ml 5x transfer buffer
   - 200ml ethanol
   - 600ml dH20

5. TBS-T
   - 100ml 10x TBS
   - 900ml dH20
   - 1ml of tween

10x TBS:

- 24.g Tris
- 80g NaCl
- Dissolve in 600ml dH20
  - o Adjust pH to pH7.6
- Make up to 1L

Table C1: List of Equipment used.

Equipment	Company	Catalogue #	Country	City
ChemiDoc XRS+ system	Biorad	170-8265	South Africa	Sandton
Direct Detect card	Merck	DDAC00010-GR	USA	Massachusetts
Direct Detect Spectrometer	Merck	DDHW00010-WW	USA	Massachusetts
Fluoroskan Ascent Microplate Fluorometer	Thermo Fisher	51119200	USA	Massachusetts
Leica Autostainer XL automated staining machine	Lecia biosystems	ST5010	Germany	Wetzlar
Leica microtome	Lecia biosystems	RM 2125 RT	Germany	Wetzlar
Leica paraffin embedding station.	Lecia biosystems	EG1150 H	Germany	Wetzlar
Tissu-Tek II tissue processor	Sakura Finetechnical	4634	Japan	Tokyo
low-fluorescence polyvinylidene fluoride (LF PVDF)	Biorad	162-0174	South Africa	Sandton
Mini-Protean Tetra Cell	Biorad	165-8004	China	Shanghai
Nikon camera	Nikon	DS-Fi2	Japan	Tokyo
Nikon Eclipse microscope	Nikon	E4000	Japan	Tokyo
Polytron homogenizer	Kinematica	PT 2100	Switzerland	Lucerne
Powerpac 300	Biorad	165-5051	China	Shanghai
Trans-Blot Turbo Transfer System	Biorad	170-4155	China	Shanghai

Table C2: List of reagents used.

Reagent	Company	Catalogue #	Country	City
10 % Na-deoxycholate	Sigma-Aldrich	D6750	New Zealand	Auckland
10 % NP-40	Sigma-Aldrich	74385	Switzerland	Buchs
10% SDS	Sigma-Aldrich	L3771	Japan	Tokyo
2-Mercaptoethanol	Biorad	161-0710	China	Shanghai
40% acrylamide solution	Merck	1.00640.1000	Germany	Darmstadt
Alcohol	Ilovo	.500	South Africa	Merebank
APS	Sigma-Aldrich	A3678	Japan	Tokyo
BLUeye Prestained Protein Ladder	GeneDireX	PM007-0500	China	Beijing
Bromophenol blue	Merck	SAAR1437500LB	South Africa	Modderfontein
Chloroform	Merck	102444	USA	Massachusetts
Clarity ECL substrate	Biorad	170-5061	South Africa	Sandton
Cover slips	Lasec	GLAS2C9M2250REC	South Africa	Cape Town
Cyclohexane	Merck	102822	USA	Massachusetts
di-Sodium hydrogen phosphate anhydrous (Na_2HPO_4)	Sigma-Aldrich	S3139	Switzerland	Buchs
doxorubicin hydrochloride	LKT laboratories	D5794	USA	St Paul
DPX	Sigma-Aldrich	6522	Spain	Madrid
DTNB	Sigma-Aldrich	D21820	USA	St Louis

EDTA	Sigma-Aldrich	EDS	Germany	Steinheim
Eosin	Lecia microsystems	3801600E	England	Peterborough
Formaldehyde	Merck	1.04003.25000	Germany	Darmstadt
Glutathione reductase	Sigma-Aldrich	G3664	USA	St Louis
Glycerol	Merck	SAAR2676520LC	South Africa	Modderfontein
Glycine	Sigma-Aldrich	G8898	China	Shanghai
GSH standard	Sigma-Aldrich	G4251	USA	St Louis
Haematoxylin	Sigma-Aldrich	MHS16	USA	St Louis
HCl	Merck	SAAR3063040LP	South Africa	Modderfontein
M2VP	Sigma-Aldrich	69701	USA	St Louis
methanol	Merck	1.06009.2500	Germany	Darmstadt
NaCl	Merck	1.06404.0500	Denmark	Hellerup
NADPH	Sigma-Aldrich	N6758	USA	St Louis
NaF	Merck	1.93270.0500	India	Mumbai
Paraffin wax	Sigma-Aldrich	P3558	USA	St Louis
Picrosirius red	Sigma-Aldrich	365548	USA	St Louis
PMSF	Sigma-Aldrich	93482	Switzerland	Buchs
Protease Cocktail	Roche	11873580001	Switzerland	Basel
Rapamycin	LKT laboratories	R0161	USA	St Paul
Slides	Lasec	GLAS4S22M3000F	South Africa	Cape Town

Sodium Orthovandate (Na_3VO_4)	Sigma-Aldrich	s6508	India	Karnataka
Sodium phosphate diabasic	Sigma-Aldrich	S3264	USA	St Louis
Sodium phosphate monobasic monohydrate ($NaH_2PO_4.H_2O$)	Sigma-Aldrich	S8282	USA	St Louis
TCE	Sigma-Aldrich	J54801	Japan	Tokyo
TEMED	Sigma-Aldrich	T9281	China	Shanghai
Transfer buffer	Biorad	10026938	USA	Hercules
Tris base	Merck	648310	China	Shanghai
Tween20	Sigma-Aldrich	P1379	USA	St Louis
Xylene	Merck	1.08633.4000	Germany	Darmstadt